Cosmic ray contribution to environmental dose rates with varying overburden thickness

Kennedy Munyikwa

IFAQ Department, Free University of Brussels, Pleinlaan 2, B-1050 Brussels, Belgium.
(Present address: Sint Jansstraat 122, B-2910 Wildert, Belgium)

(Received 28 June 2000 ; in final form 13 September 2000)

Abstract: *The dynamic character of most natural depositional systems is such that the cosmic ray dose rate experienced by a buried luminescence dating sample is not static but changes with the fluctuations in the thickness of the overburden. The use of in situ (present day) cosmic ray contribution rates assumes instantaneous deposition of the sedimentary column overlying the sample followed by a period of non-deposition. Where the cosmic ray dose constitutes a major component of the total dose (which may be up to 60 %), as is the case with many quartz aeolian dune sand systems, the assumption of instantaneous deposition may introduce notable errors. By reconstructing the burial history of a sample from the top downwards, methodology can be formulated for estimating the true cosmic ray dose received. Two different scenarios are discussed: i) gradual burial in a single depositional episode and ii) burial by episodic (multiple) increase of overburden.*

Introduction

The dose rate contribution of cosmic rays to palaeodoses for luminescence dating of geological materials varies with changes in the thickness of the overburden. The majority of geological systems are dynamic such that cosmic ray dose rates for buried samples are seldom fixed, unless the overburden thickness remains static. Although this is well known, there has been little published work which attempts to evaluate the cosmic ray dose received by a sample over its burial history allowing for changes in cosmic ray dose rate that arise from variations in overburden thickness. Cosmic ray contribution rates quoted in many publications are obtained using the method of Prescott and Hutton (1988, 1994) and estimate contribution rates at specified depths. In some cases estimation is carried out using gamma ray spectrometry (Stokes et al., 1997). In most of the cases where the cosmic ray dose rates are evaluated using these two methods, the cosmic ray contribution rates correspond to in situ (present-day) contribution rates. This would effectively be accordant with the assumption that deposition of the sedimentary column overlying the sample was in an instantaneous episode. Alternatively, some workers find it convenient to use 'token' values for cosmic ray dose rates, typically in the range 0.14 - 0.15 mGy/yr. In this paper, methodology for estimating cosmic ray contribution is applied in two scenarios where cosmic ray contribution rates are not fixed: a single step gradual accumulation of overburden and a multi-step episodic accumulation of sediment.

Nature of cosmic Rays

Cosmic rays reaching the earth dominantly comprise protons, helium nuclei and heavier particles. Electrons and gamma rays account for a minor proportion. The origin of the cosmic rays is not known with certainty but a major component is widely believed to be produced by supernovas (Friedlander, 1989). When the nuclear cosmic rays collide in the atmosphere pi-mesons are produced and these decay rapidly into muons and neutrinos. The muons decay into electrons and additional neutrinos. For purposes of buried samples, it is the flux of muons that determines the cosmic ray dose rate because of their greater penetration depth. For a comprehensive discussion of the dependence of cosmic ray dose rate with depth and expressions for evaluating contribution rates at specified depths, see Prescott and Hutton (1988, 1994).

Variation of cosmic ray contribution with changes in sedimentary cover in systems with low internal dose rates

The proportion of cosmic ray contribution to dose rates for luminescence dating is generally low and frequently constitutes less than 10 % of the total dose. Thus, when calculating the total dose rate, disregarding the gradual changes in the cosmic ray dose rate that arise from variations in thickness of the overburden, i.e. essentially assuming that the in situ (present-day) dose rates have been effective from the beginning, may not necessarily introduce large errors. However, in aeolian dune sand systems whose

Table 1: *Examples of dosimetry for samples collected from quartz dune sands with low internal dose rates (K, U & Th) and high cosmic ray contribution ratios.*

Source	Locality	Depth (m)	Lab No.	K %	K_2O %	U ppm	Th ppm	TSAC (Bq/kg)	Cosmic ray dose rate Gy/ka	Total annual dose rate Gy/ka	**Cosmic ray contribution as % of total dose rate**	Method used for determining cosmic ray dose rate
Thom et al., 1994	Eastern Australia	1-2	W1007	0.05				14.0 ±4	0.15	0.495	**30 %**	fixed approx[1]
Thom et al., 1994	Eastern Australia	1-2	W1008	0.05				11.7 ±4	0.15	0.452	**33 %**	fixed approx
Thom et al., 1994	Eastern Australia	1-2	W1015	0.07				10.3± 4	0.15	0.443	**34%**	fixed approx
Nanson et al, 1993	Simpson Desert Australia	2.0	W1310	0.57				19.1	0.15	1.163	**13%**	fixed approx
Chen, 1995	W. New South Wales, Australia	2.5	W1381	0.245 ±0.005				16.0± 0.5	not specified	0.701 ± 0.05	-	not specified
Rendell et al., 1993	Negev Desert, Israel	1.0	SH1.1	0.32 ± 0.05		0.61 ± 0.07	1.14 ± 0.21		not specified	0.919 ± 0.101	-	not specified
Stokes et al., 1997	N.E. Kalahari, southern Africa	0.5	1004/A		0.17 ± 0.01	0.5 ± 0.10	1.0 ± 0.15		0.21	0.54 ± 0.06	**39%**	in situ γ-ray[2] spectroscopy
Stokes et al., 1997	N.E. Kalahari, southern Africa	0.5	1005/A		0.08 ± 0.003	0.5 ± 0.07	1.2 ±0.11		0.20	0.46 ± 0.03	**43%**	in situ γ-ray spectroscopy
Stokes et al., 1997	N.E. Kalahari, southern Africa	2.0	1005/D		0.08 ± 0.003	0.7 ±0.13	1.3 ± 0.19		0.14	0.46 ± 0.05	**30%**	in situ γ-ray spectroscopy
Stokes et al., 1997	N.E. Kalahari, southern Africa	1.8	952/3		0.03 ± 0.001	0.5 ± 0.13	1.5 ± 0.17		0.18	0.43 ± 0.05	**42%**	in situ γ-ray spectroscopy
Stokes et al., 1997	N.E. Kalahari, southern Africa	5.0	1004/J		0.16 ± 0.001	0.6 ± 0.09	1.9 ± 0.22		0.10	0.51 ± 0.06	**20%**	in situ γ-ray spectroscopy
Stokes et al., 1997	SW Kalahari, southern Africa	3.5	942/1		0.08 ± 0.02	0.4 ± 0.12	1.7 ± 0.18		0.13	0.79 ±0.15	**16%**	in situ γ-ray spectroscopy
O'Connor & Thomas, 1999	E. central Kalahari, southern Afiica	0.63	Zam 95 20/2		0.02 ± 0.00	0.3 ± 0.03	1.10 ± 0.11		0.21± 0.01	0.37 ± 0.02	**57%**	Prescott and[3] Hutton, 1994
O'Connor & Thomas, 1999	E. central Kalahari, southern Afiica	1.8	Zam 95 32/1		0.01 ± 0.00	0.23 ± 0.03	0.45 ±0.05		0.18 ± 0.01	0.27 ± 0.01	**67%**	Prescott and Hutton, 1994
O'Connor & Thomas, 1999	E. central Kalahari, southern Africa	1.7	Zam 95 31/1		0.01 ± 0.00	0.22 ± 0.04	0.67 ± 0.03		0.18 ± 0.01	0.29 ±0.02	**62%**	Prescott and Hutton, 1994
O'Connor & Thomas, 1999	E. central Kalahari, southern Africa	1.85	Zam 95 24/1		0.03 ± 0.00	0.29 ± 0.03	1.32 ± 0.03		0.17 ± 0.01	0.37 ±0.02	**46%**	Prescott and Hutton, 1994

[1]Fixed approximation- standard fixed cosmic ray dose estimated to be contributed to each sample regardless of depth, altitude or geomagnetic latitude.
[2]In situ γ-ray spectroscopy - estimation of present-day cosmic ray contribution rate at ambient sample depth carried out in the field.
[3]Prescott and Hutton, 1994 - estimation of present-day cosmic ray contribution rate taking into account sample depth, altitude and geomagnetic latitude.

mineralogy predominantly comprises quartz and low feldspar content, as is the case over many of the world's deserts, internal dose rates tend to be low since quartz itself does not contain significant K, U or Th concentrations. Internal dose rates (from K, U & Th) ranging between 0.16 Gy/ka and 1 Gy/ka have been reported from aeolian dune sands from the southern African Kalahari, (O' Connor & Thomas, 1999; Stokes et al, 1997; 1998; Munyikwa, et al, 2000) and the Australian Simpson Desert (Nanson et al, 1993). Such low internal does rates imply that the proportion of the total dose rate that arises from cosmic rays is significantly higher, constituting up to 50-60 % of the total dose rate at times (Stokes et al, 1998; O'Connor and Thomas, 1999) (see Table 1). In such cases inaccuracies in the estimation of the cosmic ray dose rate may introduce significant uncertainties when a sample's age is evaluated.

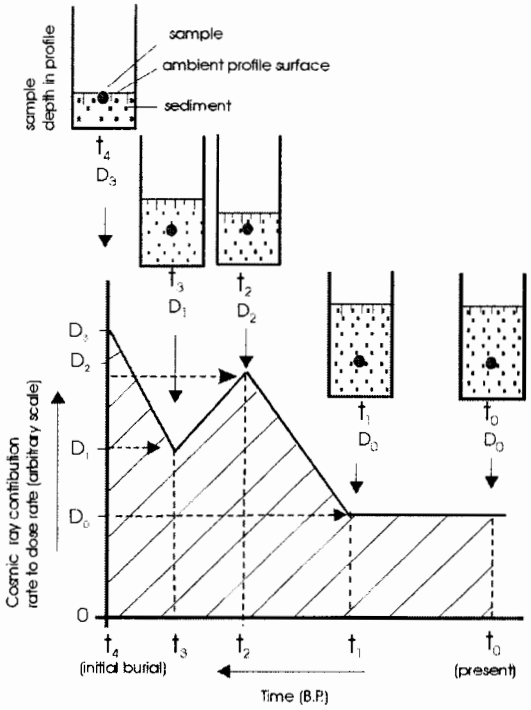

Figure 1: *Variation of cosmic ray dose rate with fluctuating depth experienced by a hypothetical buried sample. The rates of change in dose rate are not necessarily straight lines and linearity has been adopted for simplicity in this case. The various stages in the burial history of a sample at times $t_4 - t_0$ B.P. as well as the corresponding cosmic ray dose rates are also indicated. Area under curve represents total energy received.*

Storage of energy for luminescence dating purposes begins the moment a sedimentary particle is shielded from light (burial). Since penetration of cosmic rays depends on thickness of overlying sediments, the cosmic ray dose rate will vary with the rate of increase or decrease of the sedimentary cover (Figure 1). In aeolian depositional systems this rate is not necessarily linear and it may vary with geomorphic factors such as sediment supply, wind energy, topographic and climatic conditions.

Estimation of cosmic ray contribution

Cosmic ray dose received by a sample buried in a single episode at a constant depositional rate

A sample situated at the base of a stratigraphic column where the overlying sediments were deposited in a single episode at an approximately constant rate will have experienced a steady reduction in cosmic ray dose rate at a pace corresponding to the depositional rate. Depending on the sedimentation rate, such a column can either be deposited rapidly or gradually. In the case of a rapidly deposited column (Figure 2a(i)), estimating the total cosmic ray contribution by multiplying the in situ (fixed depth) cosmic ray dose rate (D_{B0}) (e.g. dose rate obtained using the method of Prescott & Hutton (1994)) by the burial age of the sample (t_2) would not significantly underestimate the true cosmic ray contribution.

Alternatively, if sediment overlying the sample is deposited gradually (at a relatively constant rate), the cosmic ray dose rate for a sample buried at the base of the column will reduce at a similarly gradual rate (Figure 2a(ii)). When the sedimentation ceases (at t_1) a period of stability may ensue during which the sample depth remains unchanged and the cosmic ray dose rate for the buried the sample stays effectively constant. Under such circumstances, the total cosmic ray dose received by Sample B (D_{CosB}^{tot}) retrieved from the base of the sediment column can be approximated by summation of the area under the curve in Figure 2a(ii) using the expression:

$$D_{CosB}^{tot} = D_{B0}t_2 + \tfrac{1}{2}(D_{B1} - D_{B0})(t_2 - t_1) \qquad (1)$$

where t_2 is the time Before Present (B.P.) since burial, t_1 is time since termination of the deposition and t_0 is the present (or 0 yr. B.P.). D_{B0} is the in situ (or current at time of sampling) dose rate and D_{B1} is the cosmic ray dose rate at time t_2 (just after burial began). Attempting to evaluate the total cosmic ray dose received by the sample by simply multiplying the in situ (fixed depth) cosmic ray dose rate by the burial age of the sample, t_2, will give a value of $D_{B0}t_2$. This effectively underestimates the true cosmic ray contribution rate by $\frac{1}{2}(D_{B1}-D_{B0})(t_2 - t_1)$. The magnitude of this underestimation relative to the total

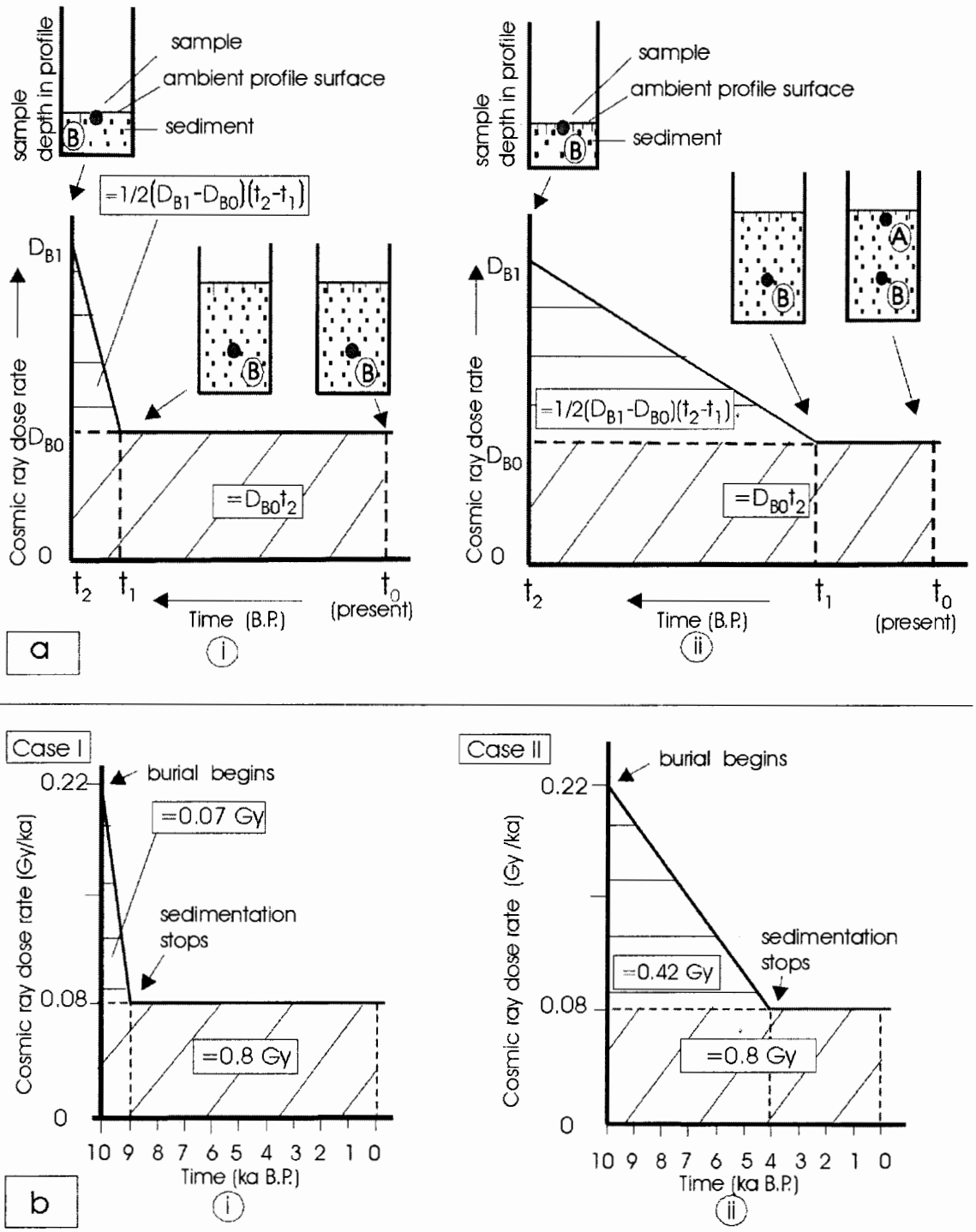

Figure 2: *(a) Sediment deposited overlying Sample B in a single depositional episode under two possible scenarios: i) rapidly ii) gradually. Cosmic ray dose accumulated depends on sedimentation rate.*

(b) Numerical illustration of variations in cosmic ray dose received by a sample at a particular site that may occur as a consequence of differences in sedimentation rate. Case (I) is characterised by rapid deposition followed by a stable phase whilst in Case (II) the deposition is more protracted.

cosmic ray dose will depend on the sedimentation rate and duration over which the sedimentation occurs (thickness of the sedimentary column).

Accordingly, if the palaeodose for Sample B is determined from the luminescence signal to be P_B, then:

$$P_B = D'_B\, t_2 + D_{B0}\, t_2 + \tfrac{1}{2}\,(D_{B1} - D_{B0})\,(t_2 - t_1) \qquad (2)$$

where D'_B is the annual dose rate from environmental radioactivity (α, β & γ) for Sample B. Expression (2) would still be difficult to solve for the burial age of Sample B (t_2) because both t_1 and t_2 are unknowns. The best manner to circumvent this problem is to reconstruct the burial history in reverse order. Thus, the first step would be to calculate the approximate date when sedimentation ceased at the top of the profile (t_1). To determine t_1, a sample is collected from just below the surface (Sample A, Figure 2a(ii)), sufficiently deep to avoid disturbances and material inhomogeneities but shallow enough to be representative of the period when sedimentation stopped. The depth of Sample A has remained fixed since it was buried, thus, the cosmic ray dose rate has been constant throughout most of the sample's burial history. If P_A is the measured palaeodose of Sample A, then:

$$P_A = (D'_A + D_{AC})\, t_1 \qquad (3)$$

$$t_1 = P_A / (D'_A + D_{AC}) \qquad (4)$$

where D'_A is the annual dose rate from environmental radioactivity for Sample A. D_{AC} is the mean annual cosmic ray dose rate evaluated using the method of Prescott and Hutton (1994).

Expression (4) can be solved for t_1 and subsequently this value (t_1) can be substituted into expression (2) to solve for t_2 (the burial age of Sample B) as below:

$$t_2 = \frac{P_B + \frac{1}{2}(D_{B1} - D_{B0})t_1}{D'_B + \frac{1}{2}D_{B1} + \frac{1}{2}D_{B0}} \qquad (5)$$

Thus, expression (5) yields a luminescence age (t_2) that allows for the variations in cosmic ray contribution rate to the palaeodose of a sample collected from a profile where the overlying sediments have been deposited in a single episode at a gradual rate. To numerically illustrate how imperative such a correction can be, consider the two hypothetical cases (I and II) of samples collected from a site located at 20° S latitude at an altitude of 1100 m a.s.l. In case I, sedimentation commences at 10 ka B.P. (Figure 2b(i)) and a column of 10 m of aeolian sands are deposited rapidly between 10 ka and 9 ka B.P. From 9 ka to 0 ka B.P. there is a phase of stability during which no deposition occurs. If the sediments are essentially quartz sands with a porosity of 30 % and a corrected density of 1.8 g/cm^3, then the calculated cosmic ray dose rate for Sample B collected from the base of this column (using the method of Presscott and Hutton (1994)), changes from 0.22 Gy/ka just after burial of the sample (ca. 10 ka) to 0.08 ka at 9 ka BP when the deposition stops. From 9 ka to 0 ka the cosmic ray dose rate is fixed at 0.08 Gy/ka. The total cosmic ray dose received by the sample can be calculated to be about 0.87 Gy. If, however, the change in cosmic ray dose rate between 10 and 9 ka that arises from the increase in overburden, is ignored and the cosmic ray contribution is calculated using the in situ (fixed) dose rate of 0.08 Gy/ka by simply multiplying this dose rate by 10 ka, a cosmic ray dose of 0.8 Gy is obtained. Ignoring the change in dose rate between 10-9 ka, thus, effectively underestimates the true cosmic ray contribution by only about 9 %. Even in cases where cosmic ray contribution constitutes about 50 % of the total dose, such an underestimation would introduce an error of less that 5 % to the age calculation.

In hypothetical case II, however, sedimentation commences at ca. 10 ka B.P. and between 10 ka and 4 ka, 10 m of dune sands are deposited at a relatively constant rate, after which a period of geomorphic stability ensues, spanning 4 ka to 0 ka B.P. Calculation using the method of Prescott and Hutton (1994) shows that just after the beginning of sedimentation (10 ka) the Sample B located at the base on the column experiences a dose rate of 0.22 Gy/ka. This dose rate will decline gradually until 4 ka, when the calculated dose rate is 0.08 Gy/ka and sedimentation ceases. From 4 ka to 0 ka BP, the dose rate for Sample B remains static at 0.08 Gy/ka. The true total cosmic ray dose received by the sample between 10 – 0 ka is 1.22 Gy. If the column is viewed as having been deposited instantaneously and the cosmic ray dose between 10-0 ka is calculated by simply multiplying the in situ dose rate by the time of burial (10 ka), a value of 0.8 Gy for the cosmic ray contribution is obtained. This underestimates the true cosmic ray contribution by 0.42 Gy. If the cosmic ray constitutes 50 % of the total dose, this underestimation would translate into a luminescence age of at least 20 % older than the true age. The magnitude of this type of error increases with

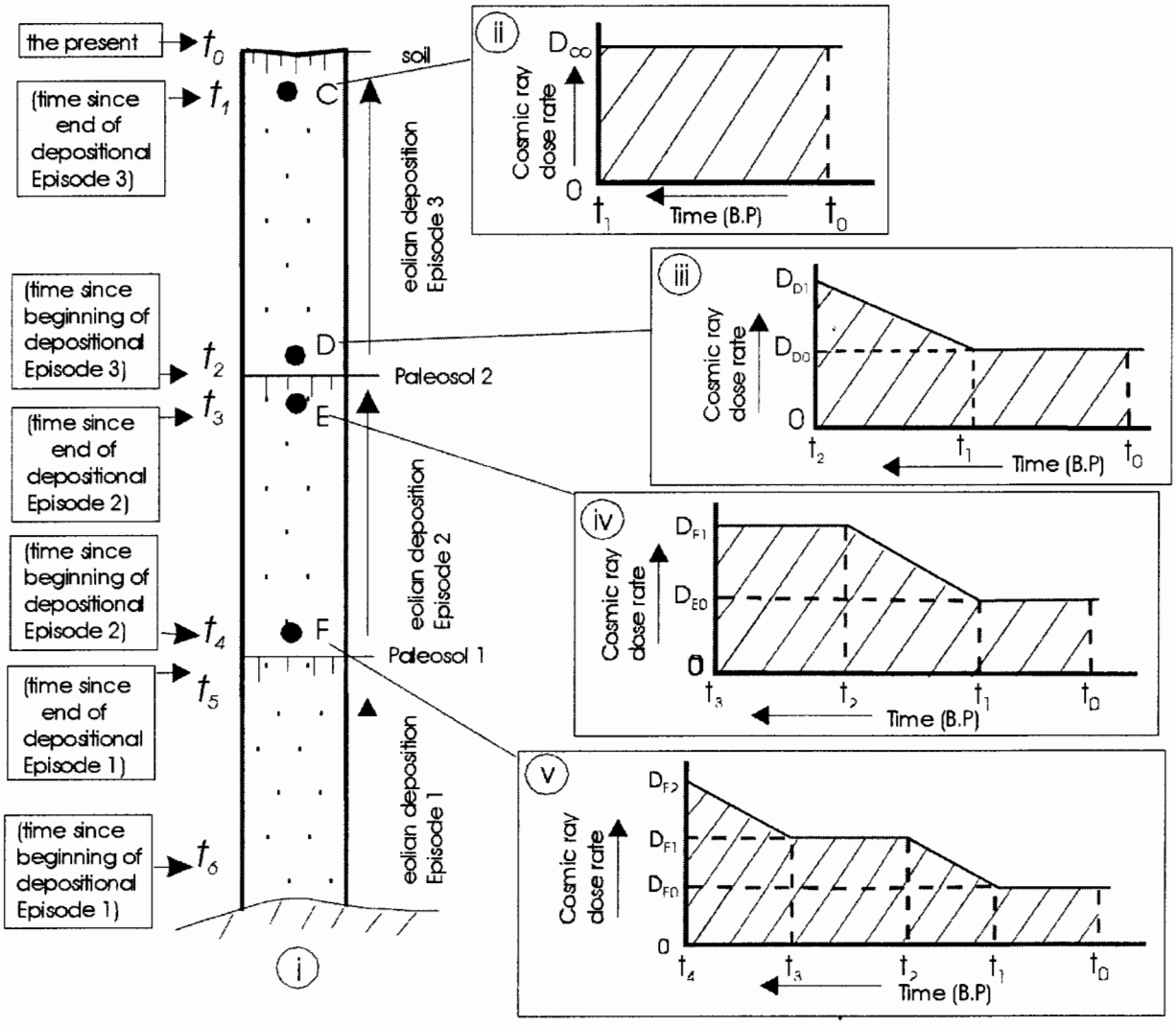

Figure 3: *Stratigraphic column resulting from multiple episodes of deposition with intervening periods of stability. Also illustrated is the evolution of cosmic ray dose contribution for samples C, D, E and F recovered from specified positions down the profile.*

proportion of the total dose rate constituted by the cosmic ray contribution.

Cosmic ray dose received by a sample buried by sediment deposited in multiple episodes

As opposed to a single gradual depositional episode discussed above, accumulation of sediments can occur as multiple events with intervening phases of stability. Figure 3(i) demonstrates a profile in dune sands that accumulate from three depositional episodes (Episodes 1, 2 &3) separated by two stable periods (Paleosols 1 & 2). As in the case of gradual burial, the total cosmic ray dose received by a sample retrieved from any part of the stratigraphic column can be approximated by a systematic reconstruction of the burial history. Accordingly, the initial step would be to determine when sedimentation ceased at the top of the profile (end of Episode 3). Sample C is retrieved from just below the surface of the sedimentary column and its depth has not changed since burial. Thus, the cosmic ray dose rate it has experienced (D_{C0}) has remained fixed between the times t_1 and t_0 (Figure 3(ii)) and is approximately equal to the in situ cosmic ray dose rate (this can be approximated using the method of Prescott and Hutton (1994)). Once the palaeodose and environmental dose rate have been determined the burial age of the sample, t_1, can be calculated and this age approximates the end of Episode 3.

Sample D is recovered from just above Paleosol 2 and its cosmic ray dose rate history is more complex than that of Sample C (Figure 3(iii)). An increase in the overburden above the sample during aeolian Episode 3 (t_2 to t_1) resulted in a corresponding reduction in cosmic ray dose rate from D_{D1} to D_{D0}. No sedimentation occurred during the period t_1 to t_0 and the cosmic ray contribution to the dose rate was static at D_{D0}. An evaluation of the total cosmic ray dose rate received by Sample D should be a summation of the area under the curve in Figure 3(iii) and both t_1 and t_2 should be known to achieve this. The value of t_1 can be approximated by the burial age of Sample C and t_2 is the burial age of Sample D. Determination of the palaeodose and environmental dose rate enables t_2 to be calculated since D_{D1} and D_{D0} can be evaluated using the method of Prescott and Hutton (1994).

Sample E retrieved from just below Paleosol 2 would yield an age that approximates the end of the depositional Episode 2 (Figure 3(iv)). Reconstruction of the cosmic ray dose rate history shows that just after burial, (t_3), the dose rate experienced by the sample remained fixed at D_{E1} until t_2. Sediments were deposited in Episode 3 from t_2 to t_1 and the cosmic ray dose rate reduced to D_{E0} after which it remained unchanged between t_1 and t_0. The total cosmic ray dose received by the sample can be approximated by summation of area under the curve in Figure 3(iv) but the times t_1, t_2 and t_3 are required to achieve this. The values t_1 and t_2 are equivalent to the ages of samples C and D respectively and the dose rates D_{E0} and D_{E1} can be evaluated using the method of Prescott and Hutton (1994). Thus, t_3 (the age of Sample E) can be calculated once the palaeodose and environmental dose rate are determined.

The burial age for Sample F, deposited at the beginning of Episode 2 (overlying Paleosol 1), can also be evaluated by similar downward reconstruction. The cosmic ray dose rate for the sample changed from D_{F2} at t_4 to D_{F1} at t_3 then remained unchanged until t_2 when it went down to D_{F0} (Figure 3(v)). The times t_1, t_2, and t_3 are equivalent to the ages of samples C, D and E respectively and the cosmic ray dose rates D_{F0}, D_{F1} and D_{F2} can be approximated using the method of Prescott and Hutton (1994). If the palaeodose and environmental dose rate are known, the age of Sample F (t_4) can be calculated.

In summary, samples collected from profiles that are deposited in multiple episodes experience a stepwise reduction in cosmic ray dose rate. The total cosmic ray dose received by a given sample can be evaluated by summing up the area under the sample's cosmic ray dose rate history curve. In principle, it should be possible to carry out similar reconstructions for cosmic ray dose received by samples recovered from stratigraphic columns where deposition has occurred in any number of episodes. As has been demonstrated, it is always imperative that the time limits of the overlying depositional episodes and hiatuses are determined before an attempt can be made to evaluate the true cosmic ray dose received by the sample. This, therefore, necessitates cautious field procedures and the recognition of stratigraphical discontinuities where they exist.

Conclusions

The use of in situ (present day) cosmic ray contribution rates as the mean cosmic ray dose rates, operational throughout the burial history of a sample, may erroneously estimate the true cosmic ray contribution in cases where the sedimentary column was not deposited instantaneously. The magnitude of this inaccuracy depends on:

(i) the fraction of the total dose constituted by the cosmic ray dose,
(ii) depositional regime (whether it is single episode, rapid, gradual or multiple episode and
(iii) the duration of the depositional phase as opposed to the stable phase.

Methodology has been presented above that demonstrates that it is feasible to evaluate the cosmic ray dose received by a sample that is overlain by a sedimentary column deposited in a single, gradual depositional episode or episodically with intervening periods of stability. It is imperative to note that the evaluation is achieved by reconstructing the deposition of the column from the top downwards. This implies that sampling has to be done systematically, with samples collected above and below any evident discontinuities in deposition (e.g. paleosols).

This discussion has only considered cases where the sedimentary environment is purely depositional. Environments that involve intermittent erosional and depositional phases would imply a rising and falling cosmic ray dose rate and the accurate evaluation of such a cosmic ray contribution would be a more complex procedure. However even is such cases, there would be little justification for the use of in situ cosmic ray dose rates as the mean dose rates throughout the burial histories of the samples unless the deposition of the sedimentary column above the sample was relatively rapid.

References

Freidlander, M.W., (1989). *Cosmic rays.* Harvard University Press, Cambridge, Mass., pp160.

Munyikwa, K., Van den Haute, P., Vandenberghe, D. and De Corte, F., (2000). The age and palaeoenvironmental significance of the Kalahari Sands in western Zimbabwe from a thermoluminescence reconnaissance study. *In press.*

Nanson, G., Chen, X.Y. and Price, D. M., (1995). Aeolian and fluvial evidence of changing climate and wind patterns during the past 100 ka in the western Simpson Desert, Australia. *Palaeogeography, Palaeoclimatology, Palaeoecology*, **113**, 87-102.

O'Connor, P.W. and Thomas, D.S.G., (1999). The timing and environmental significance of Late Quaternary linear dune development in western Zambia. *Quaternary Research*, **52**, 44-55.

Prescott, J.R. and Hutton, J.T., (1988). Cosmic ray and gamma ray dosimetry for TL and ESR. *Nuclear Tracks and Radiation Measurements*, **14**, 223-227.

Prescott, J.R. and Hutton, J.T., (1994). Cosmic ray contributions to dose rates for luminescence and ESR dating: Large depths and long term time variations. *Radiation Measurements*, **23**, 497-500.

Prescott, J.R. and Stephan, L.G., (1982). The contribution of cosmic radiation to the environmental dose for thermoluminescence dating. *PACT*, **6**, 17-25.

Rendell, H.M., Yair, A. and Tsoar, H., (1993). Thermoluminescence dating of periods of sand movement and linear dune formation in the northern Negev, Israel. In: Pye K. (ed) *The dynamics and environmental context of eolian sedimentary systems.* Geological Society Special Publication No. 72 pp 69-74.

Stokes, S., Thomas, D.S.G. and Washington, R., (1997). Multiple episodes of aridity in southern Africa since the last interglacial period. *Nature*, **388**, 154-158.

Stokes, S., Haynes, G., Thomas, D. S. G., Horrocks, J. L., Higginson, M. and Malifa, M., (1998). Punctuated aridity in southern Africa during the last glacial cycle: The chronology of linear dune construction in northeastern Kalahari. *Palaeogeography, Palaeoclimatology, Palaeoecol*ology, **137**, 305-322.

Thom, B., Hesp, P., Bryant, E., (1994). Last glacial "coastal" dunes in Australia and implications for landscape stability during the Last Glacial Maximum. *Palaeogeography, Palaeoclimatology, Palaeoecology*, **111**, 229-248.

Reviewer

J.R. Prescott

Red thermoluminescence (RTL) in volcanic quartz: development of a high sensitivity detection system and some preliminary findings

Morteza Fattahi and Stephen Stokes

Oxford Luminescence Research Group, School of Geography, University of Oxford, Mansfield Road, Oxford OX1 3TB.

(Received 15 October 2000 ; in final form 10 November 2000)

Abstract: *As part of a general study exploring the suitability of the RTL of quartz for dating volcanic events, a modified Risø Reader apparatus has been assembled and tested. Modification consisted of an alternative, cooled photomultiplier, and the incorporation of signal pass filters which have not previously been employed in RTL investigations. The use of an extended S20 9650 PMT provides a greater quantum efficiency in the wave range 600-800 nm than the traditionally used 9635 bialkaline tube. A substantially disadvantage of using such an extended tube relates to the relatively high thermal background generated with the photocathodes. To overcome this limitation we have tested the PMT response via cooling down by c. -17°C. This reduced the background to an order of magnitude (~ 200 c/s). A cooled (~-17°C) extended S20 Photomultiplier (PMT) demonstrated a signal increasing and background decreasing due to PMT cooling up to 400°C. A range of filter combinations was examined by both empirical experiments of RTL on quartz extracted from a late Holocene, New Zealand dune sand sample ($OX_{OD}847/3$) and a uv-vis spectrophotometer. Of the filter combinations examined, a Hoya 2-63 and Schott BG-39 provided the best IR suppression and therefore signal to noise ratio. However, as the BG-39 limits a substantial component of the 600-620 nm RTL peak emission , it may be inadequate for relatively young or insensitive samples. In such cases a new IR suppression filter (Corion FR-400S) is recommended.*

Introduction

Red Thermoluminescence (RTL) in quartz was first observed in samples collected from volcanic ash layers (Hashimoto et al., 1987). Since that time RTL in quartz has attracted considerable attention (e.g., Hashimoto et al., 1991, 1996; Pilleyre et al., 1992; Miallier et al., 1991, 1994 a, b). Previous research conducted on the RTL peak in quartz is summarised in Table 1. Unlike the more commonly employed ultra-violet and blue quartz TL emission bands which bleach readily in daylight, and occur frequently in quartz from a wide variety of geological settings, RTL has been recognised dominantly in quartz of volcanic origin and is only slightly sensitive to daylight bleaching (Miallier et al., 1994c). As a consequence, quartz RTL has been considered a potentially useful dosimeter for the dating of thermal resetting events (e.g., volcanic eruptions, baking of sediments & flint).

Despite over a decade of research into RTL of volcanic and other quartz, and the production of a small (<20) number of palaeodoses which have resulted in age estimates that compare favourably to independent age control, a number of important questions and research directions remain outstanding. These include:

1. The need for a systematic test of photomultiplier (PMT) and filter combinations in order to maximise RTL signal to noise.

2. Usually analysis of RTL, particularly of high (>300 °C) temperatures, has been complicated by high thermal background (e.g. Scholefield and

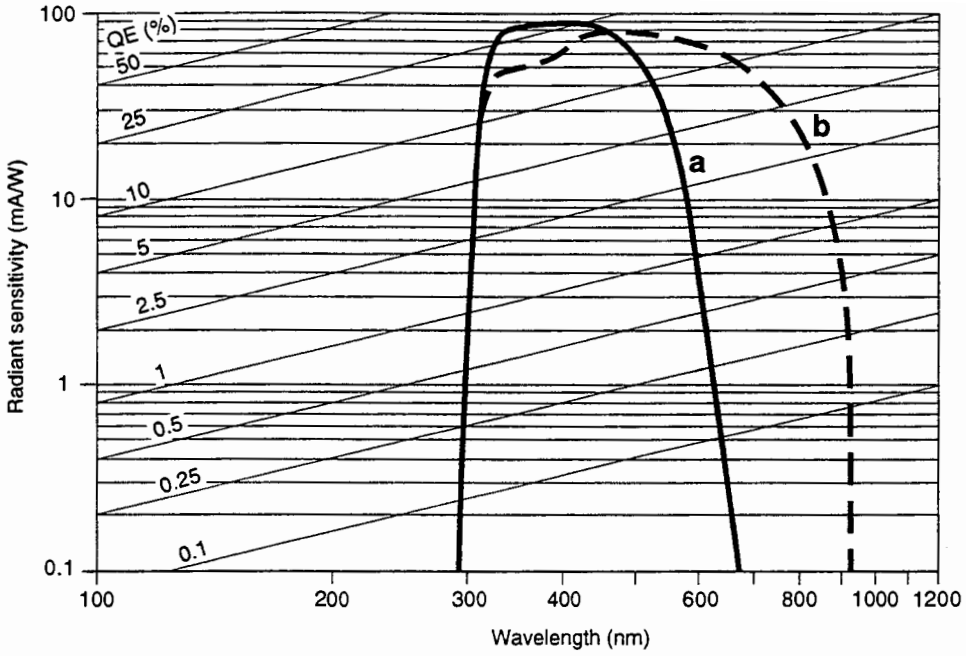

Figure 1. Quantum efficiency of Electron Tubes 9635Q and 9658 PMTs. Data from PMT catalogue.

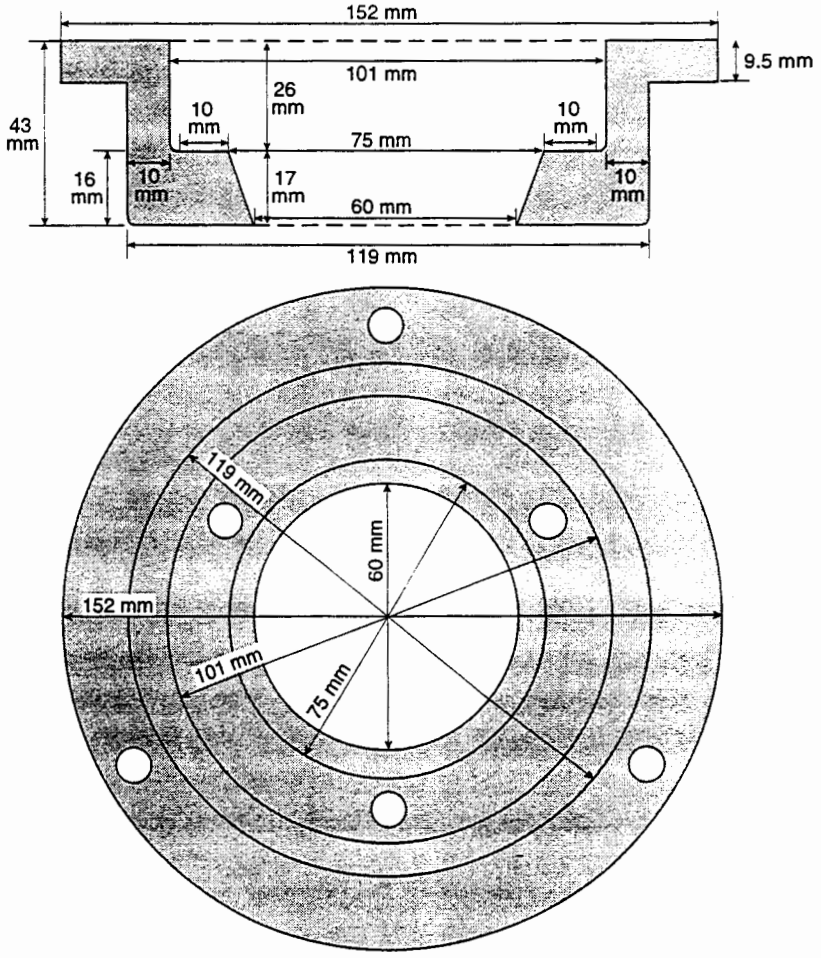

Figure 2. Adapted flange, which locates the S20 tube above the standard RISO OSL/IRSL collar.

Prescott, 1999). This has limited scope of RTL analysis typically to <450°C. While this is capable of primarily useful age-related information (e.g. Montret et al., 1992), the potential of higher temperature traps remains generally unknown.

3. The need for a survey of RTL for a range of volcanic deposits over a full (0-500°C) range of glow curves temperatures. Use of high (>300 °C) temperature peaks has to a large degree been prohibited by high temperature background and correspondingly poor signal to noise ratios (e.g., Scholefield and Prescott, 1999).

4. Tests on the potential of optical stimulation of the trap responsible for RTL.

5. The need for further systematic study of the thermal and optical stability of the RTL traps in quartz to complement existing research.

We have initiated a project, which seeks to explore additional physical aspects of RTL in quartz and assess its potential for dating volcanic deposits. Our approach was to first assemble and test apparatus to detect RTL in quartz, and it is subsequently intended to quantify some aspects of RTL properties in detail (peak temperature, dose effects, thermal stability, life time preheating and annealing effects, etc). This paper summarises the initial stages of the project, including an overview of the photomultiplier and filter combinations which we have tested.

The photo detection system

While bialkaline tubes such as the EMI 9635Q have great utility for detecting UV-blue emission and have also been employed in RTL studies (e.g., Miallier et al., 1991), they have poor quantum efficiency at longer wavelengths (Figure 1). The S20 Trialkali (Na-K-Sb-Cs) tube (EMI 9658B) offers a response from UV to near IR, which is particularly suitable for the detection of red luminescence. In collaboration with Mr Henrik Christiansen (Risø labs) we have attached an S20 PMT to a Risø model TA-15a Automated TL/OSL reader (Bøtter-Jensen, 1997). A flange was designed that locates the S20 tube above the standard Risø OSL/IRSL collar which is fitted with a focussing lens system (Figure 2). This arrangement allows routine operation of the RISO reader while the red tube is mounted.

A disadvantage of the S-20 PMT is its relatively high dark count at room temperature (c. 2 kc.s^{-1}). This thermally-generated dark count can be reduced by an order of magnitude to levels comparable to that of a bialkali tube by active cooling down to ~ -15°C (Figure 3). For this purpose we use an S 600 PHOTOCOOL Thermoelectric Refrigerated Chamber. Maximum cooling (~Δ40°C) can be achieved with 1 hour of switching on, while the warm-up cycle takes the order of 3 hours.

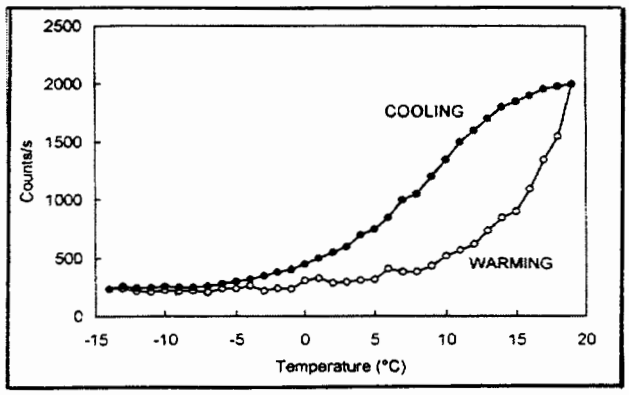

Figure 3. S20 PMT background versus photocathode temperature. Dark count was detected by combination of FR-400S+OG-590 filters.

Active cooling dramatically reduces the PMT background at low (<380°C) temperatures. At higher temperatures, somewhat surprisingly, the PMT background is greater for the actively cooled PMT than for the same PMT held at room temperatures. The response of the PMT increase by approximately factor of 2 which results in an enhanced level of black body radiation at TL measurement temperatures which exceed c. 300°C (Figure 4, Table 2). It is noted that the temperature at which the PMT background increases is different for each PMT temperature used (@ -17.7°C significant increases start at 300°C; @ 20°C significant increases start at 360°C). Actual RTL measurement show a similar enhancement (Figure 5, Table 3) which results in an enhanced signal to noise (S/N) ratio for glow curve temperatures below 350°C (Table 4). Above that glow curve temperature there is no specific S/N advantage, but the enhanced count rate of the cooled tube is advantageous.

Table 1. Selected previous research conducted on the RTL peak in quartz

Authors	Deposits studied	PMT/filter combination	Comments
Hashimoto et al. (1987-1991-1993-1994-1996)	Natural quartz of dune sand, granite and fossil bones	R649 (Hamamatsu Photonics Co, Japan)/ IR cut-off filter (IRA-05) R-649	Red emission band at 330°C, at 620 nm (heating rate 1°C/s) was used for dating fossil bones, finding the relation between RTL and impurities, Colour images of different deposits
Kanemaki et al. (1991)	Volcanic Glass Fractions from tephra (Japan)	R649 (Hamamatsu Photonics Co, Japan)/ (Toshiba 0-58) 580 nm (Ealing 35-5420) 640 nm	Red emission band at 330°C, at 620 nm (heating rate 1.7°C/s). They attributed this to Quartz and Plagioclase microcrystals
Liritzis et al. (1996)	Materials extracted from a pyroclastic formation and consists of quartz which sets the boundary to the heterogeneous material of volcanic origin	EMI 9635 QA/ A blue filter and an IR rejection filter to detect 325°C peak of TL	Four samples were dated successfully. The mean age was 1460 (±460, ±595) yr B.C
Miallier et al. (1991-1994)	Xenolithic quartz grains heated by Volcanic Products of Gravenoire Volcano (France)	EMI 9635 QA/ ORIEL 610 FS RG610 (Schott)	A band at 380-395°C , at 610-620 nm (heating rate 5°C/s) was used for exploring the properties of quartz and dating Pumice eruption up to half a million years
Pilleyre et al. (1992)	Sediments heated by lava-flows (France)	EMI 9635 QA/ RG610 (Schott)	A band at 380-395°C, at 610-620 nm (heating rate 5°C/s). Samples 10-150 ka were dated successfully
Rendell et al.(1994)	Synthetic, hydrothermal, and volcanic quartz (England)	PMT(200-800nm)	3-D spectral measurements demonstrated: Red peaks at 135°C, 280°C, 400°C (heating rate 2.5°C/s)
Scholefield et al. (1999)	Samples of quartz extracted from a variety of sediments	EMI 9635 QA and EMI 9558 Q/	3-D spectral measurements demonstrated: Red peaks at 135°C(1.96 eV), 205°C(1.97 eV), 305°C(2.00 eV) and355°C(2.05 eV) (significant red at ~1.9 ev/650nm) heating rate 5k/s

Optical filter combinations

In designing filter combinations for RTL measurements, we have attempted to maximise luminescence transmission of 600-620 nm (Hashimoto et al., 1987; Miallier et al., 1991), while minimising passage of other photons (in particular photons which contribute substantially to thermal (blackbody) radiation). We have tested a range of filter combinations by both measuring transmission windows using a uv-vis spectrophotometer, and conducting empirical experiments of RTL on quartz extracted from a late Holocene, New Zealand dune sand sample ($OX_{OD}847/3$). The sample was collected from within a suite of prograding coastal dune features within the Bay of Plenty area, North Island, New Zealand. Construction of these dunes has occurred following the post Glacial sea level rise due to an abundance of volcanic detritus supplied (via coastal erosion and fluvial transportation) from the adjacent acid Taupo Volcanic Zone.

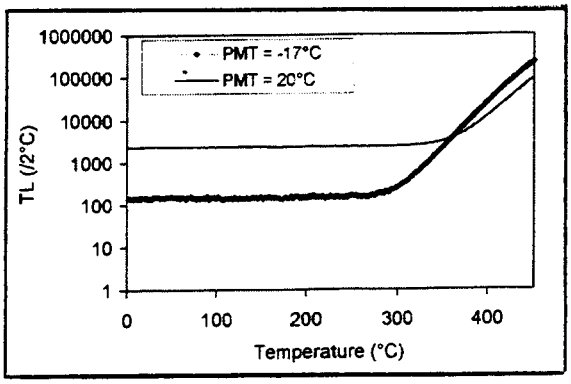

Figure 4. Dark count of a blank aluminium disc on RISO (0-450°C, heating rate 2°C.s^{-1}). Measurements are repeated 10 times while PMT temperature set to (1) 20°C and (2) -17°C. Average of measurements are showed for each experiment. Dark count was detected by combination of FR-400S+OG-590 filters.

The filters tested are primarily those which are widely available and in use in TL laboratories. Three heat rejection filters were incorporated in our tests (Table 5). The HA-3 and BG-39 are widely employed in TL and OSL applications for long cut filtering and heat rejection (Aitken, 1998). We additionally tested a multi-layer laminated, Corion FR-400S filter which according to the manufacturers possesses a sharp long cut at around 700 nm. This particular filter is supplied as a 52mm square which was cut down to the necessary 45mm diameter of the RISO filter holder. Corion produce a range of other small diameter (25mm) long and short pass filters which are potentially useful for RTL applications, but these have not been investigated at this stage due to the reduction in signal pass which would result from their size. There are a range of long pass filters capable of restricting wavelengths shorter than c. 600nm. Of these we have chosen to examine the characteristics of the Hoya 2-63, 3-67, and 2-61 and Schott OG-590 and RG-610 filters.

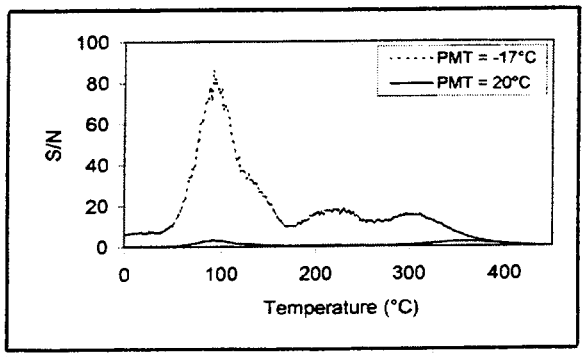

Figure 5. Average artificial TL measurement on RISO (0-450°C, heating rate 2°C .s^{-1}) of sample 847/3 after ~ 42 Gy dose. Measurements are repeated 3 times while PMT temperature set to (1) 20°C and (2) -17°C.

Spectrophotometer analysis

All spectrophotometer measurements were undertaken at room temperature on a Shimadzu uv-vis spectrophotometer model P/N 204-58000. Examination of the long cut filters reveals strong contrasts between filters (Table 5). While the HA-3 filter offers a broad transmission window passing from UV to red at levels in excess of 60%, its high (20%) transmission in to the IR renders it of limited utility for RTL studies. Of the two other filters tested the BG-39 offers the best (i.e., lowest) IR transmission characteristics, but transmits only c. 50% of that passed by the FR-400S in the red region of interest (c. 600-640 nm; Table 5).

Detailed examination of the FR-400S long cut characteristics has identified two minor IR pass window at around 720 and 900 nm. While the high signal pass levels are advantageous in RTL studies,

Table 2. Summary of dark noise measurements at different PMT temperatures.

Temp (°C)/ratio	Low temp. Average $_{(0\text{-}100°C)}$ dark noise (/2°C)	High temp. (@ 400°C) dark noise (/2°C)
-17.7	145.8	26046.8
20	2374.3	12466.6
-17.7/20	0.06	2.09

Table 3. Summary of sample 847/3 TL measurement at different PMT temperatures.

Temp (°C)/ratio	$TL_{(50\text{-}150)}$	$TL_{(350\text{-}450)}$
-17	325533	1324642
20	211707	623569
-17/20	1.5	2.1

Table 4. Ratio of signal TL to background (S/N) at different temperatures for sample 847/3 + β =40Gy.

Temp (°C)	$S/N_{(100)}$	$S/N_{(200)}$	$S/N_{(300)}$	$S/N_{(350)}$	$S/N_{(400)}$	$S/N_{(420)}$	$S/N_{(440)}$	$S/N_{(450)}$
-17.7	77.16	15.97	15.44	6.90	1.27	0.56	0.12	0.03
20	3.02	0.47	0.69	2.21	1.25	0.60	0.15	0.05

Table 5. Spectral characteristics of some long cut filters

Filters (mm)	Peak Transmission		IR Transmission		Heat Rejection
	%	λ (nm)	%	λ(nm)	
HA-3 (3)	~ 80	340-620	>20	700->900	Poor
BG-39 (2)	~ 80	450-530	~ 0.2	760-900	Good
	~ 60	540-580			
	~ 30	580-620			
	~ 8	620-640			
BG-39 (1)	~40	400-580	~0.5	700-720	Good
	~30	580-620	~0.1	720-760	
	~15	620-660	~0.1	860-900	
FR – 400S (7)	~ 70	440-600	~ 2.0	700-720	Medium
	~ 60	600-640	~ 0.5	720-740	
	~ 10	680-700	~ 0.3	760-900	

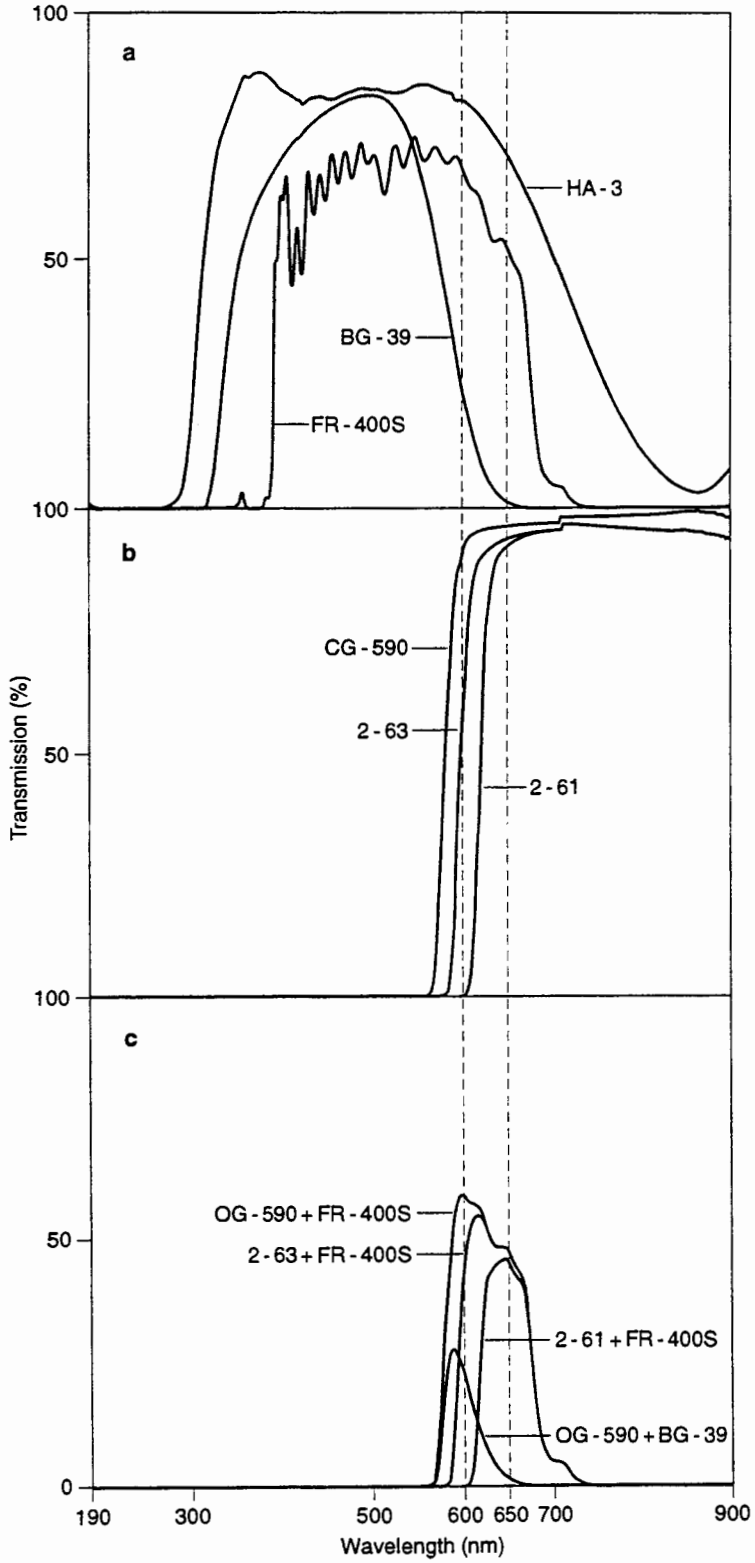

Figure 6. *Filter combination of long cut and short cut filters.*

Table 6. Spectral characteristic of combination of selected filters

Filters	Max Peak Transmission %	λ (nm)	Min-Max Wavelength λ (nm)
FR-400S + OG-590	60	600-620	570-730
FR-400S + 2-63	52	610-630	580-730
FR-400S +2-61	46	630-650	600-730
FR-400S +3-67	46	570-620	550-730
FR-400S + RG 610	44	620-640	590-730
BG-39 + OG-590	34	590-610	570-720
BG-39 +2-63	29	600-620	580-720
BG-39 +2-61	18	620-640	600-720
HA-3 + OG-590	60	610-630	530-900
BG-39 + RG 610	12	610-630	590-720
BG-39(1)+HA-3 + OG-590	20	580-600	560-720
BG-39(2)+HA-3 + OG-590	21	580-600	560-670
BG-39(1) + HA-3 + 2-63	12	600-620	580-710
BG-39(2) + HA-3 + 2-63	16	600-620	580-670
BG-39(1) + HA-3 + 2-61	8	620-640	600-710
BG-39(2) + HA-3 + 2-61	3	620-630	610-670
BG-39(1)+FR-400S+OG-590	14	590-610	570-680
BG-39(2)+FR-400S+OG-590	19	580-600	560-770

Table 7. Luminescence transmission characteristic of combination of selected filters

SC filter (mm)	LC filter (mm)	$TL_{50\text{-}150}$	$TL_{300\text{-}430}$	$BG_{50\text{-}150}$	$BG_{300\text{-}430}$	$TL_{390/110}$	$S/N_{(50\text{-}150)}$	$S/N_{(300\text{-}430)}$
OG-590 (2)	HA-3 (4)	1571241	4755374	10354	46278692	3.03	151.75	0.10
OG-590 (2)	BG-39 (2)	136070	353917	9019	63855	2.60	15.09	5.54
OG-590 (2)	FR-400S	325533	1324642	7382	2756975	4	44.09	0.48
2-61 (3)	HA-3, BG-39 (1)	188177	462180	9767	250566	2.46	19.27	1.84
2-63 (3)	BG-39 (2)	136381	406312	9326	51254	2.98	14.62	7.93
2-63 (3)	BG-39 (1)	38162	28065	67323	65721	0.74	0.57	0.43
2-63 (3)	FR-400S	418629	886934	19091	2501796	2.12	21.9	0.35
2-61 (3)	BG-39 (2)	29200	52503	10709	38118	1.80	2.73	1.38
2-61 (3)	HA-3 (4)	652287	477286	10240	45168705	0.73	63.70	0.01

these IR pass window complicate sample stimulation by IR.

The results for filter combinations are summarised in Figure 6. Of these the combination of FR-400S and OG-590 provide the greatest red transmission while limiting the principle IR transmission to levels lower than c. 720nm (Table 6). We note additionally, that in testing for phosphorescence or other malign effects, the orientation or ordering of the filters had no significant effect on the transmission window.

Actual RTL measurements using various filter combinations

To confirm the general patterns noted above we tested a range of filter combinations using a quartz sample which has been demonstrated to exhibit no significant TL sensitivity changes during repeated measurements (Fattahi and Stokes, 2000). An aliquot of the sample 847/3 was repeatedly given a c. 42 Gy test dose and its RTL measured (heating rate 2°C.s^{-1}) after changing the filter combination.

As it is shown in Table 7 the combination of 2-63(3mm) + BG- 39 (2mm) posses the best S/N at $TL_{300-430}$ (7.93) and the best ratio of $TL_{390/110}$ (2.9). The combination of HA-3 and Long pass filters demonstrated the poorest S/N at $TL_{300-430}$ (0.01) and the lowest ratio of $TL_{390/110}$ (0.73) and the highest S/N at TL_{110} (152). The combination of HA-3 + BG-39 + 2-61 demonstrated a poor S/N at $TL_{300-430}$ (1.84).

Conclusions

Quartz RTL has been considered a potentially useful dosimeter for dating volcanic deposits. In order to maximise RTL measurements, we have adapted a RISO model TA-15 Automated TL/OSL reader to a suitable apparatus to detect RTL in quartz. We have specifically tested a cooled (~-17°C) extended S20 and a range of filter combinations. The best combination found was the Schott OG-590 and Corion FR-400S filters. While these provide an enhanced signal level, the limited pass of 700-720 nm photon leaded to high (>1MC. S^{-1}) background at elevated (>450°C) temperatures.
Specific observations we have made include:

1- By cooling the Red PMT (~-17°C) background decreases at low (<380°C) temperatures and increases at high temperatures.
2- Signal increases due to PMT cooling.
3- S/N increases at temperatures lower than 400°C and decreases at higher temperatures (up to 0.03 @450°C).
4- A Corion FR-400S IR suppresser filter increases signal levels by comparison to the more commonly used Schott BG-39 (~100%), although the latter has better IR >700 nm rejection.
5- Of the various combinations of short cut and long cut filters tested via spectrophotometer, OG 590 and FR- 400 S provides the greatest red transmission while limiting the principle IR transmission to levels lower than c. 740 nm .
6- RTL measurements demonstrated that the combination of 2-63(3mm) + BG- 39 (2mm) posses the best S/N at 300-430°C (7.93) and the combination of OG-590 and FR- 400 S provide the best S/N at (200-300) °C (~30).
7- Filter orientation or ordering of the filters is not significant.

So, for measuring RTL of old or sensitive samples the combination of BG-39+2-63 is ideal. For RTL measurements on young or insensitive samples or studies, which are exploring the dating potential of the bleachable RTL, peak (Scholefield et al., 1999 in press; Fattahi and Stokes, 2000) a combination of OG 590 and FR- 400 S would appear more suitable.

We have adjusted our system within the structural limitations of the RISO reader to optimise the detection of RTL emission. While this represents a significant development on apparatus previously used to detect RTL we would welcome any additional comments or advice, which practitioners may have. On the basis of our spectral observations on the HA-3 filter we would further suggest that it performs a limited function in TL (and OSL) applications. To minimise black body emission for either bialkaline or extended red tubes such as the S-20 there would appear to be little merit in using this filter in preference to a BG-39 or similar filter (e.g., Schott BG-38).

Acknowledgements

We are grateful to the ongoing advice and assistance of Lars Bøtter-Jenson and Henrik Christiansen (Risø), Finn Jacobsen (PFR Denmerk), Dr Richard Bailey and Martin Franks (RLAHA, Oxford). MCHE of Islamic

Republic of Iran are thanked for financial support to Morteza Fattahi.

References

Bøtter-Jensen L. (1997) Luminescence technique: Instrumentation and methods. *Radiation Measurements* 27, 749-768.

Fattahi M. and Stokes S. (2000) Extending the time range of luminescence dating using red TL (RTL) from volcanic quartz. *Radiation Measurements* 32, 479-485.

Hashimoto T., Yokosaka K. and Habuki H. (1987) Emission properties of thermoluminescence from natural quartz - blue and red TL response to absorbed dose. *Nuclear Tracks and Radiation Measurements* 13, 57-66.

Hashimoto T., Sakai T., Shirai N., Sakaue S. and Kojima M. (1991) Thermoluminesence spectrum changes of natural quartzes dependent on annealing treatment and aluminium-contents. *Analyt. Sci.* 7, 687-690.

Hashimoto T., Yokosaka K., Notoya S., Ojima T. and Sakaue S. (1993) Dependence of red thermoluminescence on Eu-anomaly in natural quartzes. *Nuclear Tracks and Radiation Measurements* 21, 209-215.

Hashimoto T., Sakaue S., Aoki H. and Ichino M. (1994) Dependence of TL-property changes of natural quartzes on aluminium contents accompanied by thermal annealing treatment. *Radiation Measurements* 23, 293-299.

Hashimoto T., Sakaue S., Notoya S., Arimua. and Konishi M. (1996) Changes in Luminescence color images from quartz slices with thermal annealing treatments. *Radiation Measurements* 26, 233-242.

Liritzis I., Michael C. and Galloway R.B. (1996) A significant Aegean volcanic eruption during the second millenium B.C. revealed by thermoluminescence dating. *Geoarchaeology* 11, 361-371.

Miallier D., Faïn J., Montret M., Pilleyre T., Sanzelle S. and Soumana S. (1991) Properties of the red TL peak of quartz relevant to thermoluminescence dating. *Nuclear Tracks and Radiation Measurements* 18, 89-94.

Miallier D., Faïn J., Sanzelle S., Pilleyre T., Montret M., Soumana S. and Falguères C. (1994) Attempts at dating pumice deposits around 580 ka by use of red TL and ESR of xenolithic quartz inclusions. *Radiation Measurements* 23, 399-404.

Miallier D., Sanzelle S., Falguères C., Faïn J., Montret M., Pilleyre T., Soumana S., Laurent M., Camus G. and De Goër de Hervé A. (1994) Intercomparisons of red TL and ESR signals from heated quartz grains. *Radiation Measurements* 23, 143-154.

Miallier D., Faïn J., Montret M., Pilleyre T., Sanzelle S. and Soumana S. (1994) Sun bleaching of the red TL of quartz: preliminary observations. *Ancient TL*, 12 No1.

Montret M., Miallier D., Sanzelle S., Faïn J., Pilleyre T. and Soumana S.TL (1992) Dating in the Holocene using red TL from quartz. *Ancient TL*, 10.

Pilleyre TH., Montret M., Faïn J., and Sanzelle S. (1992) Attempts at dating ancient volcanoes using the red TL of quartz. *Quat. Sci. Rev.* 11, 13-17.

Rendell H.M., Townsend P.D., Wood R.A. and Luff B.J. (1994) Thermal treatments and emission spectra of TL from quartz. *Radiation Measurements* 23, 441-449.

Scholefield R.B.and Prescott J.R. (1999) The red thermoluminescence of quartz: 3–D spectral measurements. *Radiation Measurements* 30, 83-95

Reviewer

D. Miallier

Comments

Systematic research on the RTL of quartz seems to be fully justified because this signal has already proved to have remarkably reproducible features whatever the geographical origin of the quartz. Since it seems that difficulties of measuring this signal hinders generalisation of its use, the technical data given by Fattahi and Stokes are very welcome.

The use of sodium lamps for low-intensity laboratory safelighting for optical dating

N.A. Spooner, D.G. Questiaux and [1]M.J. Aitken

Environmental Geochemistry and Geochronology, Research School of Earth Sciences, Australian National University, Canberra, A.C.T., 0200, Australia
[1]Le Garret, 63 930 Augerolles, Puy-de-Dome, France

(Received 14 November. 2000; in final form 30 November. 2000)

Abstract *The choice of laboratory illumination for use with optical dating samples involves a compromise between minimising the unwanted bleaching of light-sensitive signals while providing sufficient visibility to allow efficient and safe workplace practice. Described here is a laboratory safelight fulfilling these requirements. The safelight module consists of a low-pressure sodium vapour lamp enclosed within a filtered and shuttered housing, and provides low-intensity (< 1 $\mu W/cm^2$) yellow-orange light, predominantly from the well-known 589.0 and 589.6 nm sodium D-lines.*

Introduction

Following the introduction by Hütt et al. (1988) of a novel means of optical dating utilising infrared-stimulated luminescence (IRSL) from feldspar minerals, a practical source of illumination was required to provide laboratory lighting that would not significantly bleach near-IR and visible-light-sensitive dating signals. Hütt et al. (1988) had avoided near-IR and the longer-wavelengths of visible light and instead utilised low-intensity blue light for safelighting, based on a consideration of the visual response of the human eye to low light levels.

However, studies of the bleaching response of feldspar luminescence (subsequently reported in Spooner 1993, 1994b) showed that even at low-intensities the blue wavelengths are effective at bleaching OSL and IRSL, and earlier work on the TL bleach spectra of feldspar (Krønborg, 1983) had revealed that short-wavelength (<550nm) visible light bleached the 330°C TL of K-feldspar, and Spooner et al. (1988) showed similar behaviour for quartz. An ideal laboratory safelight should be conveniently usable with these minerals, hence a source deficient in both blue/UV and IR was sought. Previous recipes for laboratory safelighting, by Sutton and Zimmerman (1978), Jensen and Barbetti (1979), Spooner and Prescott (1986), Smith (1988) and Galloway and Napier (1991), were variations on filter-wrapped or coloured fluorescent tubes, which emit strongly in the blue and also produce some very-low-visibility emissions > 700nm. An alternative means of isolating an orange-red waveband (Lamothe 1995), rejects both shorter and longer offband wavelengths using IR-absorbing "detector trimmer" glass in conjunction with Lee 106 red filter, passing red light of approximately 600-650 nm.

However, although orange-red/red wavelengths are not greatly less effective in bleaching the feldspar luminescence than yellow-orange, they are less visible to the observer. Indeed, the human eye is a critical factor in safelight selection, responding strongly to both light intensity and colour and exhibiting two intensity-dependent regimes - photopic (cone-dominated) and scotopic (rod-dominated) vision. The transition from photopic to scotopic vision (the Purkinje effect) occurs at about 1 lumen/m^2, which for 555 nm light corresponds to about 150 nW/cm^2, but the threshold varies between people, not least by reason of age. Photopic vision has peak response at 555 nm, with 10% points at about 475 nm and 650nm, and 1% points at about 430 nm and 685 nm, with the limits for visibility lying at about 390 nm and 780 nm.

The photopic response curve is approximately symmetric, and as the efficiency of bleaching both quartz and feldspar by visible light decreases monotonically with increasing wavelength, safelight wavelengths should be chosen from the long-wavelength wing of the photopic curve as these bleach less for equivalent visibility than the same optical power flux of shorter wavelength illumination. The scotopic response curve has similar form to the

photopic, but shifted approximately 50 nm to shorter wavelengths, hence below the photopic-scotopic transition red is even less visible relative to green-orange than it is in the photopic regime. Consequently red wavelengths are not ideal if very low illumination intensities are sought, and the waveband range of 555-630 nm (corresponding to 100%-25% relative to peak photopic response) represents the optimal compromise between visibility and minimal bleaching.

Choice of light source took into account the ease of selection of this desired waveband, and factors such as cost, general availability, operator safety, reliability and lifetime. Low-pressure sodium lamps fulfil the practical criteria and emit the majority of their radiant energy in the sodium D doublet at 589.0 and 589.6 nm, with only weak emissions in the UV/blue or near-IR wavebands, and so place minimal demands on optical filtering to remove the strongly-bleaching near-IR and UV/blue light (high-pressure sodium lamps, commonly used for example as highway lighting, emit significantly in both these wavebands and so are undesirable in this application).

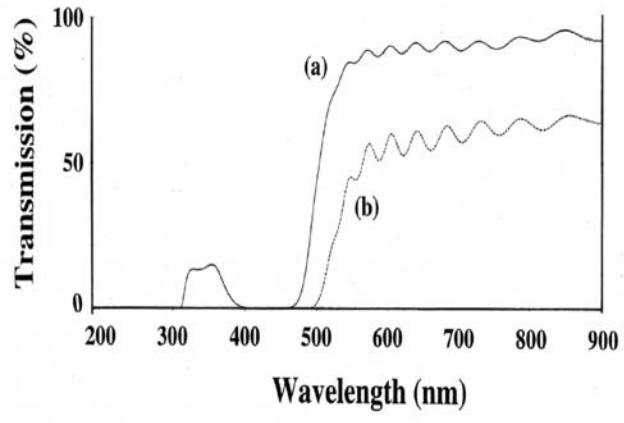

Figure 1. *The transmission spectra of (a) one layer of Lee 101 yellow filter and (b) a 5-layer stack of the same. The relatively strong attenuation of the stacked filter layers is inconsequential for visibility, as the unfiltered lamp output greatly exceeds the required illumination intensity. The distinctive "ripple" at wavelengths > 550 nm is not a measurement artefact.*

The sodium lamp illumination module

The original module, developed in 1989 by the authors at the Research Laboratory for Archaeology and the History of Art (RLAHA), Oxford, comprises one Osram MW 18W Super SOX low-pressure sodium lamp mounted within a sealed and shuttered housing of 360 mm length and 200 mm diameter. The housing is manufactured from opaque PVC tube and sealed at both ends (the ANU version is smaller for bench-top convenience, at 310 mm length and 160 mm diameter) and has the advantage of portability compared to fluorescent light fixtures.

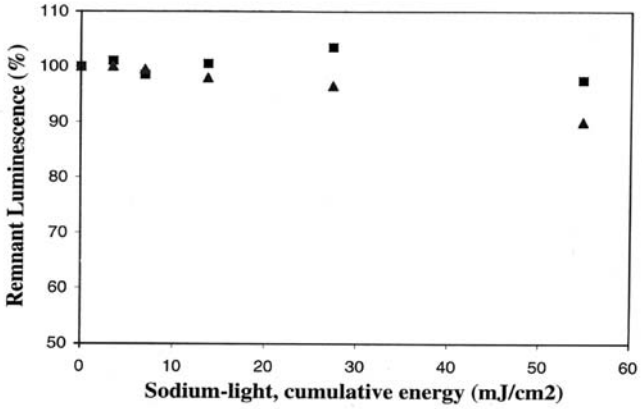

Figure 2. *Bleaching of IRSL and OSL by illumination from a sodium lamp module delivering ≈ 950 nW/cm^2 to the sample, plotted as percentage of initial intensity. Full abscissa scale corresponds to ≈ 200 hours exposure to practical working-levels of sodium light. Triangles represent IRSL from Achenheim loess. Stimulation was by 853.0 Δ 82.4 nm IR from a filtered xenon lamp set (Spooner and Questiaux, 1989), and detected by an EMI 9635QA optically filtered by one 2 mm Schott BG 39 filter, passing approximately 450-600 nm. Squares represent OSL from Chaperon Rouge quartz, with UV emissions detected following short exposures to 514.5 nm light*

Illumination emanates from one 50 x 85 mm window, elliptical in shape and of 36 cm^2 area, screened with five layers of Lee 101 yellow plastic filter. The clear aperture of the window is adjusted by a sliding opaque shutter (conveniently produced from similar tubing as used for the housing). The transmission spectra of these filters were measured at RLAHA, Oxford, and pass < 1 part in 10^4 for wavelengths < 450nm, per layer of filter plastic (50% pass at approximately 500 nm), effectively blocking the weak shorter-wavelength sodium emission lines. The transmission spectrum of 5 stacked layers of Lee 101 yellow filter is shown in Figure 1. Although the Lee 101 filter has high IR transmissivity, IR

emissions from low-pressure sodium lamps are insignificant and can be safely ignored.

Two steps are taken to improve the uniformity of illumination: a layer of Lee 216 white diffusion filter is added to the stacked Lee 101 filters to disperse the emitted beam, and then indirect illumination is obtained by targeting the module window towards the ceiling or a light-coloured wall to effectively produce a large-area dim source (so aiding retention of dark adaptation by eliminating the window as a bright "spot" source in the direct line of vision). The diffuse reflected light when the shutter is fully opened is ample for "housekeeping"; activities requiring unshielded exposure of samples are performed with the module window 90% closed by the shutter.

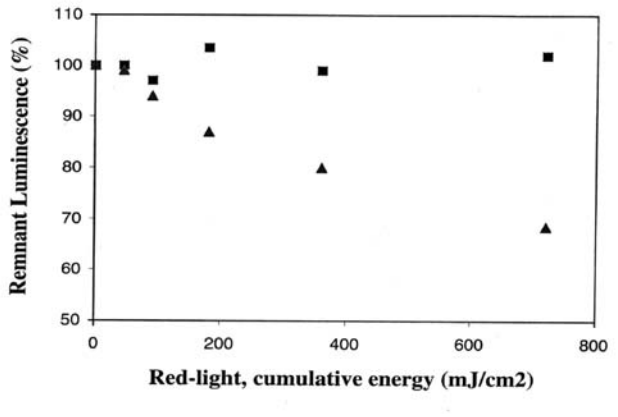

Figure 3. *Bleaching of IRSL and OSL by red illumination from fluorescent tubes wrapped with 6 layers of Lee 106 primary red, delivering ≈ 12.5 μW/cm^2. Triangles represent IRSL from Achenheim loess and squares OSL from Chaperon Rouge quartz. Measurement conditions as in caption for Figure 2. Full abscissa scale corresponds to ≈ 200 hours exposure to practical working-levels of light.*

Performance Tests

Bleaching of OSL and IRSL was assessed in two ways. Firstly, by measurement of the optical power under typical darkroom conditions followed by calculation of acceptable exposure times using bleach response data from Spooner et al. (1988) for quartz, and Godfrey-Smith et al. (1988) and later Spooner (1993, 1994a,b) for quartz and feldspar. Secondly, samples were exposed to cumulative doses of safelight and the bleaching of OSL and IRSL monitored by short exposures to IR and 514.5 nm light. We did not investigate the bleaching of TL on the assumption that the more optically-sensitive OSL and IRSL signals would better reveal any deleterious effects of the safelights.

An alternative laboratory illumination in use at RLAHA and ANU consists of 40W fluorescent light tubes wrapped in 6 layers of Lee primary red 106 filter; these were also tested (see Figure 3).

(1) Power measurements

Optical powers at typical safelight intensities were measured at various locations in the darkroom, using a large-area silicon photodiode (Radio Spares cat. # 303-674) calibrated by means of a spectrally-insensitive pyroelectric radiometer (Molectron Corporation, model PR-20). The minimum intensity for practical work under sodium lamp illumination was measured to be ≈ 2 nW/cm^2 and a comfortably-bright working level with samples exposed, obtained with the shutter 90% closed, was ≈ 100 nW/cm^2. When the shutter was fully opened the light intensity was typically ≤ 1 μW/cm^2, depending on module aspect and location in the laboratory.

Typical red-light intensities from fluorescent tubes wrapped in 6 layers of Lee 106 ranged between ≈ 0.2 μW/cm^2 and ≈ 15 μW/cm^2

Bleaching after various exposure durations at these intensities can be estimated from Figures 2 and 3, or calculated from the data sets of Spooner (1993, 1994a,b). Spooner (1994a) showed that ≈ 150 mJ/cm^2 of 589.4 Δ 8.9 nm light was required for a 5% reduction of the 514.5nm-stimulated OSL from quartz., equivalent to about 420 hours of exposure at the comfortable sodium light intensity of 100 nW/cm^2, indicating about 1% bleaching of the fast component per 3-4 days exposure at this intensity. The extent to which this slow bleaching rate gives a margin of safety to normal laboratory procedures is self-evident.

Similar measurements were reported in Spooner (1993, 1994b) for bleaching IRSL from a microcline feldspar: 43mJ/cm^2 of 589.4 Δ 8.9 nm light was required to reduce the IRSL from this sample by 10%, corresponding to about 5 days exposure to illumination of intensity 100nW/cm^2, ie., about 2%/day. Green (514.5nm) stimulated OSL from this same sample resisted bleaching by 589.4 Δ 8.9 nm light more strongly, a 10% reduction requiring 170mJ/cm^2, which corresponds to ≈ 20 days safelight exposure at ≈ 0.5%/day decay rate.

It was concluded that the time required for significant bleaching (>2%) of either quartz or feldspar OSL or IRSL at practical illumination powers far exceeds cumulative exposure times accrued in typical laboratory practice.

(2) Bleaching of quartz OSL and feldspar OSL and IRSL

The sodium lamp was tested with window fully open, and the optical power at the sample was measured as 30/10 photodiode-meter units, corresponding to ≈ 950 nW/cm^2. Red-light exposures were made underneath a red-filtered fluorescent tube at an illumination intensity of 12.5 μW/cm^2 (for comparison, we consider ≈ 100 nW/cm^2 sodium light and ≈ 1 μW/cm^2 red light to be practical laboratory illumination levels).

These experiments utilised OSL from HF-acid-etched 90-125 μm quartz (Chaperon Rouge, Morocco, sample 724g, Rhodes, 1990), and both OSL and IRSL from 4-11 μm polymineral fine-grains extracted from two loess samples (Achenheim, Germany, sample T1, Questiaux 1990, and Val Sorda, Italy, sample VS1, Accorsi et al., 1990). Natural luminescence only was used; results are shown in Figures 2 and 3.

Depletion of OSL from the Chaperon Rouge quartz was not clearly produced by either red or sodium light exposures. However, under red light the Achenheim fine-grains exhibited depletion rates of ≈ 4 %/day for IRSL, compared to ≈ 1.2 %/day under sodium lamp illumination, these rates being calculated for the above-nominated practical laboratory illumination levels for the respective lights.

Exposure of the second loess sample, VS1 from Val Sorda, Italy, to the sodium lamp module with the shutter 90% closed gave a 10% reduction of IRSL after the equivalent of 28 days exposure. This IRSL (N + beta + preheat) bleaching rate is slower than, but still in reasonable accord with, that of the Achenheim loess and comparable to those above and reported by Spooner (1993, 1994a,b).

It was concluded that red light results in a slower decay rate per unit energy, but as significantly higher powers of red light are required for similar visibility, for "real-time" exposures the sodium light is safer. While recognising that "practical" light intensity is subjective, given the individuality of eyesight, we estimate that full scale on Figures 2, 3 corresponds to 200 hours exposure at practical darkroom illumination levels.

Discussion and Conclusions

When used at very low-intensities (< 100 nW/cm^2), the 500-650 nm waveband is safe for feldspar luminescence, but only the longer portion of that waveband is advisable for use with quartz. The precise illumination intensity chosen will depend on the worker's eyesight and the nature of the procedure, noting that "pitch black" is ≈ 0.01 nW/cm^2 at 550nm, and the minimum practical intensity for seeing was measured to be ≈ 1 nW/cm^2, and a comfortable working intensity was ≈ 100 nW/cm^2.

A related issue is that of bleaching at elevated temperatures, such as when samples are removed from preheat ovens. These results, considered with Spooner (1993, 1994a) and Bailey (1998), indicate that increased bleaching efficiency at raised temperatures does not present problems at typical laboratory illumination intensities.

We note that neither the sodium lamp module nor the red light produced unambiguous depletions of 514.5 nm-stimulated OSL even over substantial exposure durations, and conclude that in practice both red-filter-wrapped fluorescent tubes and sodium lamp modules provide "safe" light conditions for preparation and manipulation of green-light-stimulated OSL samples at typical illumination intensities and durations. However, the situation appears different when red illumination is used with samples intended for IRSL analysis. Here the sodium lamp illumination is preferred on account of lesser bleaching, as well as for providing greater visual contrast, giving better visibility of objects and "sharper" perception of shadows. The principal drawback is the requirement of a 10-15 minute warm-up period for the lamp to attain full luminosity, and as this is much of the typical duration required for dark-adaptation, this delay is readily accommodated in laboratory routine.

In summary, the justification for the use of 589 nm sodium light is that the human eye sees it more efficiently and with greater visual comfort than it does red light, hence significantly less intense sodium light gives viable laboratory illumination. Practical benefits of the sodium lamp modules include easily adjustable illumination intensity, low energy consumption, and reliable, low-hazard, low-cost long-life lamps. The quality of illumination afforded by these modules, in terms of improved contrast and visual "comfort", exceeds that of red-filter-wrapped fluorescent tubes and from the perspective of many individuals, particularly older people, given that red-acuity diminishes with increasing age, they offer a means of continued and comfortable work under OSL/IRSL-safelight conditions.

Acknowledgments

We thank John Fenton for the construction of the sodium lamp modules produced at RLAHA, Jim Neale for those produced at ANU, and Cate McElroy

(RLAHA) for the IRSL measurements on Val Sorda loess.

References

Accorsi, C.A., Aitken, M.J., Cremaschi, M., Ferraris, M., McElroy, C., Questiaux, D.G., and Van Vliet Lanoe, B., (1990). The loess deposits of the Rivoli moraine system. In "The loess in Northern and Central Italy: a loess basin between the Alps and the Mediterranean region", 21-39. Editor: Cremaschi, M., ISBN 88-85329-00-4

Bailey, R. M. (1998). Depletion of the quartz OSL signal using low photon energy stimulation. *Ancient TL*, **16**, 33-36.

Galloway, R.B. and Napier, H.J. (1991). Alternative laboratory illumination: "gold" fluorescent tubes. *Ancient TL*, **9**, No.1, 6-9.

Godfrey-Smith, D.I, Huntley, D.J. and Chen, W.H. (1988). Optical dating studies of quartz and feldspar sediment extracts. *Quaternary Science Reviews*, **7**, 373-380.

Hütt, G., Jaek, I. and Tchonka, J. (1988). Optical dating: K-feldspars optical response stimulation spectra. *Quaternary Science Reviews*, **7**, 381-385.

Jensen, H. and Barbetti, M. (1979). More on filters for laboratory illumination. *Ancient TL*, **7**, 10.

Krønborg, C. (1983). Preliminary results of age determination by TL of interglacial and interstadial sediments. *PACT **9***, Part II, 595-605.

Lamothe, M. (1995). Using 600-650 nm light for IRSL sample preparation. *Ancient TL*, **13**, No.1, 1-4.

Questiaux, D.G., (1990). Optical dating of loess: comparisons between different grain size fractions for infrared and green excitation wavelengths. *Nucl. Tracks Radiat. Meas*., **18**, 133-139.

Rhodes, E.J. (1990). Optical dating of quartz from sediments. Unpublished DPhil thesis, University of Oxford, UK.

Smith, B.W. (1988). More cautions on laboratory illumination. *Ancient TL*, **6**, No.1, 9.

Spooner, N.A. and Prescott, J.R.(1986). A caution on laboratory illumination. *Ancient TL*, **4**, No.3, 46-48.

Spooner, N.A., Prescott, J.R., Hutton, J.T. (1988). The effect of illumination wavelength on the bleaching of quartz thermoluminescence. *Quaternary Science Reviews*, **7**, 325-329.

Spooner, N.A. and Questiaux, D.G. (1989). Optical Dating - Achenheim beyond the Eemian using green and infrared stimulation. In: Long and Short Range Limits in Luminescence Dating, Occasional publication No. **9**, RLAHA, University of Oxford, 97-103.

Spooner, N.A. (1993). The validity of optical dating based on feldspar. Unpublished DPhil thesis, University of Oxford, UK

Spooner, N.A. (1994a). On the optical dating signal from quartz. *Radiation Measurements*, **23**, Nos.2/3, 593-600.

Spooner, N.A. (1994b). The anomalous fading of infrared-stimulated luminescence from feldspars. *Radiation Measurements*, **23**, Nos.2/3, 625-632.

Sutton, S.R. and Zimmerman, D.W. (1978). A blue-UV absorbing filter for laboratory illumination. *Ancient TL*, **5**, 5.

Reviewer

John Prescott

Date List 7: Luminescence dates for Prehistoric and Proto-Historic pottery from the American Southwest

James K. Feathers
University of Washington, Box 353100, Seattle, WA 98195-3100 USA

(Received 25 February 2000; in final form 29 June 2000)

Introduction

This date list presents dates from over 100 ceramic and burned stone samples from prehistoric and historic sites in the American Southwest, analyzed by the luminescence laboratory at the University of Washington from 1994 to 1999. The Southwest has a rich archaeological tradition, in large part because of the remarkable preservation afforded by the generally dry climate. The detailed painted designs on much of the prehistoric pottery, the styles of which have changed rapidly through time, have also allowed a rather finely resolved chronology, tied to a calendrical scale by an abundance of radiocarbon and, particularly, tree ring dates (Blinman, 2000). Nevertheless, there are still pockets of uncertainty in Southwestern ceramic chronology. In the lowland desert region of southern Arizona, the Hohokam cultural sequence has suffered from poor resolution due to inadequacy of tree-ring dating and temporally insensitive ceramics (Dean, 1991). More relevant to this work is the poorly known chronology of the very late prehistoric/early historic record, which has recently gained interest among scholars seeking to understand the ramifications of Spanish contact on native populations (e.g., Raminofsky, 1996) and the impact of the relatively late migration to the region by Apache and Navajo groups (e.g., Towner, 1996).

The dating work reported here has not resulted from any systematic study originating from the laboratory, but rather represents the serendipitous accumulation of dating analyses contracted by a variety of academic and cultural resource management (CRM) organizations. The bulk of the dates are on Navajo ceramics or on late Puebloan ceramics, mostly from northwestern New Mexico, but also included are earlier ceramics from the Colorado Plateau, the desert lowlands of southern Arizona, and the Great Basin. Most of the dates are for pottery, but a few burned rocks from hearths and similar contexts have been included; some dates previously published are not included (e.g. Feathers and Rhode, 1998).

The analyzed ceramics are generally thin-walled (5-7mm), relatively high fired (ca. 800-900°C), and fine textured with inclusions of fine sand or volcanic material. The fine texture has necessitated use of the fine-grain dating technique. Overall the luminescence characteristics of the samples can be described as well behaved. The fabrics are composed of clays that are relatively high in naturally occurring radionuclides (means tabulated for 92 of the ceramics reported here are 12.2 ± 5.4 ppm Th and 4.2 ± 1.7 ppm U), and contain luminescent minerals of high sensitivity. Scatter in growth curves tends to be low, plateaus are generally broad, and anomalous fading is only present in a few sherds. The recovery context is often complex, representing dwellings (various pit structures, adobe room blocks or Navajo "hogans"), middens, or other activity centers, but generally radioactivity does not seem to vary greatly from different areas of the sites. Many of the ceramics were recovered from the surface. This complicates to some degree estimations of the gamma dose rate and increases the contribution from the cosmic dose rate (especially given the high altitude of some regions such as the Colorado Plateau where elevations at sites range up to 2500 m or more). However, we have shown in other contexts that these uncertainties are not greater than those for buried ceramics, particularly, as is often the case, where the timing and rate of burial are unknown (Dunnell and Feathers, 1994). Moisture contents are generally low, because of the relatively dry climate, although there is variation from place to place.

Procedures

The laboratory's procedures have evolved through the years. What follows is a generalized protocol. Sherds are broken to expose a fresh profile, and material then drilled from the center of the cross-section more than 2

mm from either surface, using a tungsten carbide drill bit. To avoid mechanical fragmentation of grains the drill is kept at low speed and material is scraped out mainly using the sides of the drill bit rather than the tip and employing minimum pressure. The material retrieved is ground gently in an agate mortar and pestle, treated with HCl and then settled in acetone for 2 and 20 minutes to separate a 1-8 μm fraction, which is then deposited onto stainless steel discs. TL is measured on a Daybreak reader using a 9635Q photomultiplier through a Corning 7-59 (blue) filter, in N_2 atmosphere, heating at 1°C/s to 450°C. A preheat of 1°C/s to 240°C and then immediate cooling to room temperature precedes each measurement. In earlier analyses, samples were preheated in a separate oven at 70°C for several days, depending to some degree on the amount of fading detected over the first few weeks. Artificial irradiation is provided by a ^{241}Am alpha source, calibrated by the manufacturer (Littlemore Scientific) following Aitken (1985), and a ^{90}Sr beta source, calibrated against a ^{137}Cs gamma source. After irradiation, sample discs are stored for at least one week prior to measurement of the luminescence.

Tests for anomalous fading involve measuring the natural signal on several discs, administering equal alpha irradiations and storing at room temperature for various times up to 8-10 weeks. The irradiations are staggered in time so that all second glows are performed on the same day. The second glows are normalized by the natural signal and the signal from the plateau region plotted against log time. Dating results of any sample showing fading beyond one week are presented as minimums, indicated in the table by italic type. Alpha irradiations were chosen for this test because of convenience in administering the dose. Moreover, for most samples, alphas are a significant contributor to the dose rate. Figure 1 shows examples of sherds displaying fading and no fading.

Paleodose is determined by combining additive dose and regeneration growth curves in the "Australian slide" method (Prescott *et al.*, 1993), using the program developed by David Huntley of Simon Fraser University. Sensitivity changes are corrected using the scale factor (which is a ratio of the two slopes) computed in that program. Where the scale factor is within two standard deviations of one, the program is run assuming no sensitivity change. Fits are either linear or, particularly for younger samples, quadratic. An earlier version of the program used a cubic rather than quadratic fit, although the cubic term for these ceramics was never significant. Dose increments are determined so that the maximum additive dose results in a signal about three times that of the natural and the maximum regeneration dose about five times the natural. A few analyses determined palaeodose by an additive dose extrapolation corrected for supralinearity by the regeneration intercept (this is indicated in the date list table and a footnote gives the ratio of the supralinearity correction to the paleodose for these few samples). One advantage of the slide method is that supralinearity is automatically taken into account, resulting in higher precision. Figure 2 shows two examples of growth curves following the slide procedure, showing samples with more and less scatter.

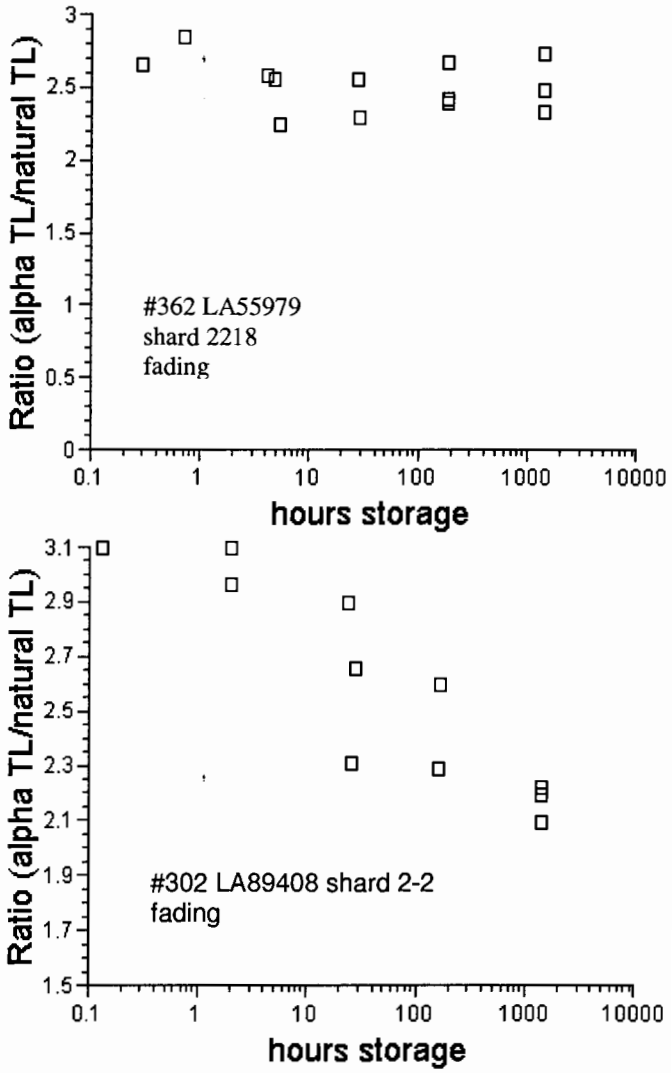

Figure 1. *Examples of anomalous fading results. (a) UW362 shows no fading over the 8-week storage time. (b) UW302 shows substantial fading that is not complete by eight weeks.*

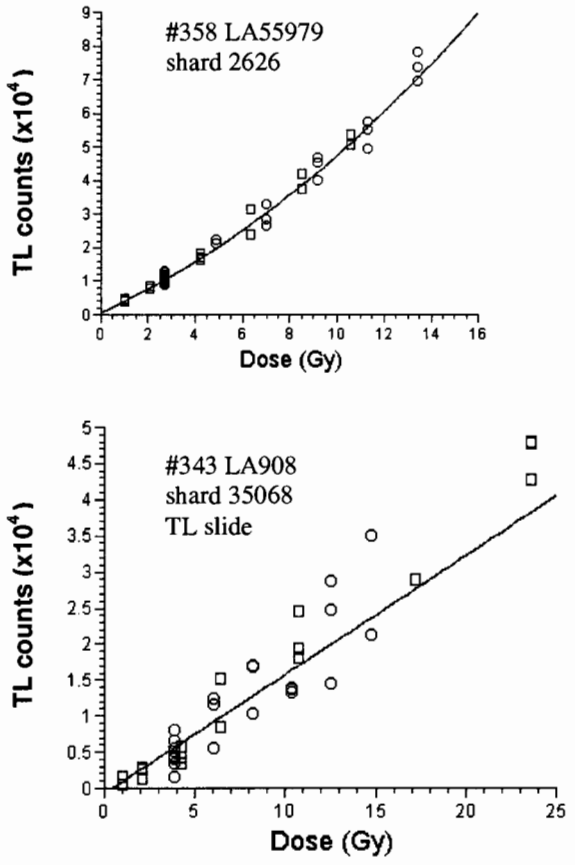

Figure 2. *(a) Quadratic fit to additive dose and regeneration points after the slide procedure for UW358. (b) Linear fit to the same kind of data for UW343, except that the scatter is much greater. In both graphs, the open circles are additive dose points and open squares are regeneration points.*

A plateau region is determined by calculating the paleodose at temperature increments between 240° and 450°C and determining over which temperature range the values do not differ significantly. This plateau region is compared with a similar one constructed for b-values, and the smaller of the two plateaus defines the region over which the signal is integrated for final determinations. Some earlier analyses defined the plateau on the basis of dose intercepts for first glows (alphas and betas) and second glows, but this more conservative approach was abandoned once more advanced slide software was obtained. Figure 3 shows some typical plateau plots.

Where the size of the sherd prevents a full multi-aliquot analysis, the palaeodose is determined by the SARA technique (Mejdahl and Bøtter-Jensen, 1994). Several aliquots are given additive doses, and then after heating to 450°C are given regeneration doses on the order of magnitude of the natural signal or the natural plus added dose signal. The apparent palaeodose is determined by regeneration measurements with each aliquot. These are plotted against the original additive dose and a linear extrapolation to the dose axis provides the correct palaeodose. We have found this method to be less precise than the multiple aliquot procedure.

A summary of procedures for deriving equivalent dose is given in Table 1.

Alpha efficiency is determined by comparing the slopes of additive dose curves built using alpha and beta irradiations. The ratio of the slopes is taken as the b-value., and this is determined by scaling the alpha curve to the beta curve using Huntley's slide program (Lian et al., 1995). A b-value variation of this program has been developed by Prof. Huntley.

Radioactivity is measured by alpha counting in conjunction with flame photometry for ^{40}K. Samples for alpha counting (for sherds, using fragments remaining after material has been removed for luminescence measurements) are crushed in a mill to a fine powder, packed into plexiglass containers with ZnS:Ag screens, and sealed for one month before counting. The pairs technique is used to separate the U and Th decay series. For flame photometer measurements, samples are dissolved in HF and other acids and analyzed by a Jenway flame photometer. K concentrations for each sample are determined by bracketing between standards of known concentration.

Both the sherd and an associated soil sample are measured for radioactivity. Additional soil samples are analyzed where the environment is complex, and gamma contributions determined by gradients (after Aitken, 1985: appendix H). The cosmic ray dose is determined after Prescott and Hutton (1988). Radioactivity concentrations are translated into dose rates following, most recently, Adamiec and Aitken (1998).

Water absorption values for sherds are determined by comparing the saturated and dried weights. For the climates typical of the Southwest, which is dry much of the year but has seasonal rain in late summer and snow at higher elevations in winter, moisture values are taken to be about 30± 20 to 50±20 percent of saturated values, depending on information provided by the archaeologist. Soil moisture contents are determined largely on the basis of texture, with values of about 6

percent for sands and 11-15 percent for siltier substrates (Brady, 1974:196).

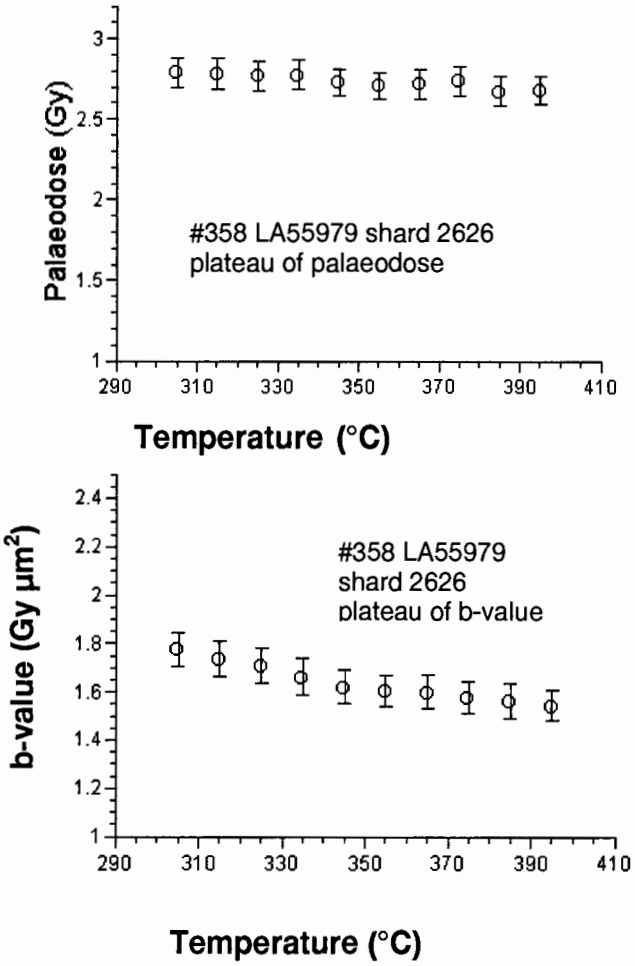

Figure 3. Plateau test for UW358 showing results for (a) equivalent dose and (b) b-value.

Accuracy and precision

Tests for accuracy are not a straight-forward task because seldom are the dating events precisely the same for luminescence and independent methods. We addressed this problem in a comparison of TL and tree-ring dates obtained from several short occupation Navajo sites in northwestern New Mexico (Dykeman *et al.*, 2000). Direct comparisons were available from 12 sites, from which 15 TL dates were obtained. The tree-ring dates were considered high quality not only because of a close match with the reference curve but because they were derived from wood containing either the outer most ring or significant amounts of sapwood. Stumps from cut limbs were available at some sites. In these cases the cutting did not kill the tree, which continued to grow (even to the present) and protected the stump rings from weathering. Distinctive axe scars, attributed to early Navajos, suggested these trees were cut during occupation. The precision of these dates was taken to be nearly 1 year. Using a 1 σ confidence interval (average 70±18 years) for the TL dates, only four of the 15 dates agreed with corresponding tree ring dates.

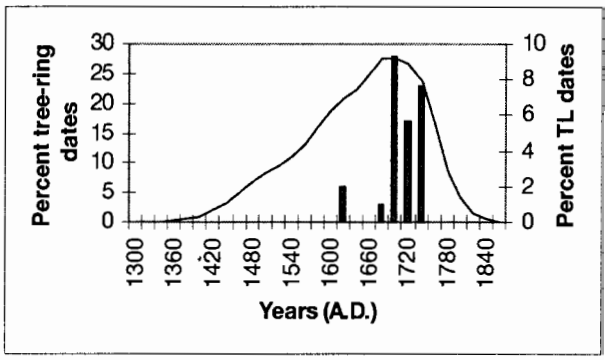

Figure 4. Comparison of aggregate TL and tree-ring dates, as explained in the text.

However, tree-rings date the cutting of a tree, usually for construction, an event that may not correspond closely with firing of the pottery. Dates of these events may differ significantly at any one site, although the differences should average out on a regional scale. Indeed, the aggregate distributions from all sites (Figure 4) show a much closer correspondence. In this figure the TL dates are treated as normal probability distributions, which are summed at any given point. The distributions from the two techniques are similar with a main node around AD 1700, although an earlier minor node apparent in the tree-ring data is less defined in the TL distribution. If the TL distribution is deconvoluted by the two ceramic types represented (Figure 5), the bimodality of one of the types closely matches the bimodality in the tree-ring dates, while both types contribute to the main node. Terminating the probability distributions of TL dates for both ceramic types at the 75th percentile produces ranges (AD 1640-1780 for Gobernador Polychrome and AD 1520-1740 for Dinetah Gray) remarkably close to the range of production estimated for both types by several radiocarbon and tree-ring dates from across the region

(AD 1630-1775 for Gobernador Polychrome and AD 1540-1800 for Dinetah Gray). These results underscore the difficulty in directly comparing dating methods that address different events, but also show that luminescence provides some chronological information -- on ceramic production -- that may not be as easily obtainable from tree-rings or radiocarbon. These data are presented in more detail by Dykeman *et al.* (2000). In a more recent study (Dykeman, 2000), a comparison of tree-ring dates (used as the standard) with 14 TL dates (numbers 357-370 in this date list) and several radiocarbon dates, all obtained from Morris I, a large Navajo site in northwestern New Mexico, concluded TL provided better accuracy and even better precision than radiocarbon. The latter suffers in this region from old wood effects and for this time period from multiple intercepts on the calibration curve.

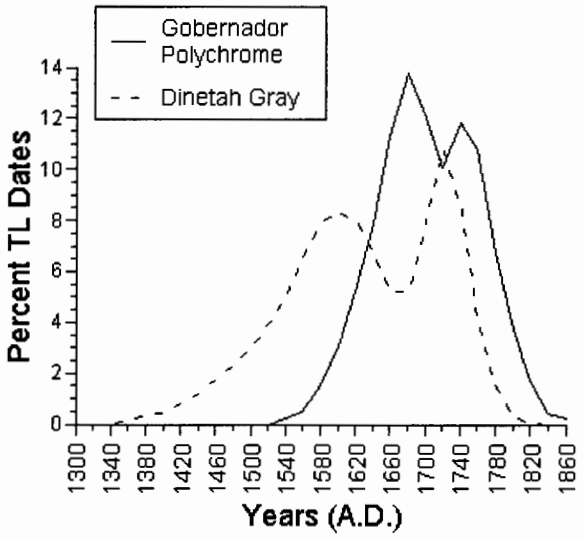

Figure 5. *Distribution of TL dates by ceramic type.*

Variable precision in the dates reflects in large part the scatter about the growth curves. As our fitting procedures and other aspects of the protocol have improved through the years, the precision obtainable has improved and become less variable. The mean, standard deviation and median of percent errors for all the dates are 12.8, 8.2 and 10.2 respectively, while the same numbers for dates obtained since 1996 are 10.7, 3.6, and 9.5 respectively. The errors reported were computed using an Excel spreadsheet developed in this laboratory and modeled after Aitken (1985: Appendix B). The errors, computed at 1σ, include both random and systematic contributions.

References

Adamiec, G., and Aitken, M. J. (1986) Dose rate conversion factors: update. *Ancient TL* **16,** 37-50.

Aitken, M. J. (1985) *Thermoluminescence Dating.* Academic Press, London.

Blinman, E. (2000) The foundations, practice and limitations of ceramic dating in the American Southwest. In *It's About Time*, edited by S. E. Nash, pp. 41-59. University of Utah Press, Salt Lake City.

Brady, N. C. (1974) *The Nature and Properties of Soils.* Macmillan, New York.

Dean, J. S. (1991) Thoughts on Hohokam chronology. In *Explaining the Hohokam: Prehistoric Desert Peoples of the American Southwest*, edited by G. Gumerman, pp. 61-149. University of New Mexico Press, Albuquerque.

Dunnell, R. C., and Feathers, J. K. (1994) Thermoluminescence dating of surficial archaeological material. In *Dating in Exposed and Surface Contexts*, edited by C. Beck, pp. 115-137. University of New Mexico Press, Albuquerque.

Dykeman, D. D.(2000), Accuracy and precision in archaeological dating: a correlation of tree-ring, thermoluminescence and radiocarbon techniques. Paper given at the 65th annual meeting of the Society for American Archaeology, Philadelphia.

Dykeman, D. D., and Wharton, J. T. (1996) Preliminary report on the Morris Site 1 Early Navajo Land Use Study and the Plan for Phase 3 – focused data recovery. Manuscript with the Navajo Nation Archaeology Department.

Dykeman, D. D., Towner, R.H., and Feathers, J. K. (2000) Tree-ring and thermoluminescence dating: evaluating methods for confidently dating protohistoric Navajo sites. *American Antiquity*, submitted.

Feathers, J. K., and Rhode, D. (1998) Luminescence dating of protohistoric pottery from the Great Basin. *Geoarchaeology* **13,** 287-308.

Kotyk, E. M., Matthews, M., Wheelbarger, L., and Skoglund, D. (undated) The Manuel Canyon settlement patterns inventory: Archaic, early Anasazi, Navajo and historic occupations. San Juan College Research Papers in Anthropology No. 11. San Juan College Cultural Resources Management Program, Farmington, NM.

Lian, O. B., Hu, J., Huntley, D. J., and Hicock, S. R. (1995), Optical dating studies of Quaternary organic-rich sediments from southwestern British Columbia and northwestern Washington State. *Canadian Journal of Earth Sciences* **32,**1194-1207.

Mejdahl, V., and Bøtter-Jensen, L. (1994) Luminescence dating of archaeological materials using a new technique based on single aliquot measurements. *Quaternary Geochronology* **13,** 552-554.

Prescott, J. R., Huntley, D. J., and Hutton, J. T. (1993) Estimation of equivalent dose in thermoluminescence dating – the *Australian slide* method. *Ancient TL* **11,** 1-5.

Prescott, J. R., and Hutton, J. T. (1988) Cosmic ray and gamma ray dose dosimetry for TL and ESR. *Nuclear Tracks and Radiation Measurements* **14,** 223-235.

Ramenofsky, A. F. (1996) The problem of introduced infectious disease in New Mexico, 1540-1680 A.D. *Journal of Anthropological Research* **52,** 161-184.

Ramenofsky, A. F. (2000) Decoupling archaeology from history: northern New Mexico. Proceedings of the Chacmool Conference, in press.

Ramenofsky, A. F., and Feathers, J. K. (2000) Ceramics, tree rings and luminescence: estimating terminal abandonment from the Lower Chama region. *Journal of Archaeological Method and Theory*, submitted.

Reed, A. D., and Zier, C., eds. (2000) The Trans Colorado Pipeline Archaeological Mitigation Project, manuscript prepared by Alpine Archaeological Consultants, Inc., Montrose, Colorado, and Centennial Archaeology, Inc., Fort Collins, Colorado for the Office of Archaeology and Historic Preservation, Denver. See site reports for Broken Vessel site (5ME4970), Aldasoro site (5MN4270), Simpson Wickiup site (5SM2425), Schmidt site (5MN4253), Oak Hill site (5MN2628), and Kennon Decker site (LA86094) by R. A. Greubel, J. D. Cater, and A. D. Reed.

Rice, G. E. (1998) Structuring the temporal dimension for Tonto Basin prehistory. In *A Synthesis of Tonto Basin Prehistory: the Roosevelt Archaeological Studies, 1989-1998*, edited by G. E. Rice, pp. 11-32. Anthropological Field Studies 41, Office of Cultural Resource Management, Department of Anthropology, Arizona State University, Tempe.

Rhode, D. (1994) Direct dating of brownware ceramics using thermoluminescence and its relation to the Numic spread. In *Across the West: Human Population Movement and Expansion of the Numa*, edited by D. B. Madsen and D. Rhode, pp. 124-132. University of Utah Press, Salt Lake City.

Towner, R. H., ed. (1996) *The Archaeology of Navajo Origins*. University of Utah Press, Salt Lake City.

Reviewer
I.K. Bailiff

DATE LIST 7: LUMINESCENCE DATES ON PREHISTORIC AND PROTO-HISTORIC POTTERY FROM THE AMERICAN SOUTHWEST

The data presented include procedures for determining palaeodose (Table 1), information about the samples and submitting organizations (Table 2), notes on abbreviations used, and the main date list (Table 3).

***Table 1**: Procedures for determining palaeodose*

Procedure	Steps
TL slide (TL1)	1. Aliquot allocation and dosing: 1-15, natural then alpha dose for fading; 16-30 natural, then regeneration doses; 31-45 natural plus added beta; 46-60 natural plus added alpha. Number of aliquots adjusted for smaller samples. 2. Preheat 240°C @ 1°C/s, and cool. 3. Heat to 450°C @ 1°C/s to measure TL, repeat for background 4. Use slide program to determine plateau. 5. Integrate over plateau region and use slide to determine palaeodose (D_E) and alpha efficiency.
TL additive dose (TL2)	1. Steps 1-3 of TL1 2. Use additive dose extrapolation to determine plateau 3. Integrate over plateau region and determine D_E by adding intercepts of additive dose and regeneration. Alpha efficiency determined as in TL1
SARA	1. Make as many aliquots as possible: some naturals, some additive dose (beta and alpha). Use same preheat and temperature regime as TL1. 2. Follow TL1 steps as much as possible, and determine a regeneration dose that yields a TL signal close in magnitude to the natural 3. Use that dose plus the additive dose to determine a regeneration dose for various additive dose discs 4. Use additional regeneration doses as needed to bracket the natural or additive dose signal. 5. Determine apparent D_E of natural and additive dose discs by interpolation 6. Use apparent D_E as function of original additive dose to extrapolate D_E 7. If D_E from SARA and D_E from the limited number of discs for TL1 agree, use weighted average
OSL	1. Use single aliquot protocol, after Duller (1995). Steps are preheat, natural OSL, dose, preheat, OSL, dose, preheat, OSL, etc., using at least 5 dose increments, then several preheats and OSL measurements without dose to correct for signal loss at each step. 2. Build additive dose and regeneration curves for different aliquots and combine using slide after normalization by the natural signal. Regeneration followed heating to 450°C 3. Preheat at each incremental step at 220°C for five minutes @1°C/s 4. OSL measured at 100°C using green light from filtered quartz-tungsten halogen lamp (550 ± 20nm). Stimulate for 5s at reduced lamp intensity.

Table 2: Sample information

Sample reference	Sample Type	Region	Contracting Agency	References
344-346,348, 350-351, 430	Ute ceramics	Colorado Plateau (N. Mex. and Colo.)	Alpine Archaeological Consultants, Montrose, CO	Reed and Zier, 2000
349	Navajo ceramic			
347	Puebloan ceramic			
230-233	Hohokam ceramics	Tonto and Phoenix Basins (Ariz.)	Arizona State University, Tempe	Rice, 1998
135-138	Navajo ceramics	Colorado Plateau (N.Mex.)	Cultural Resources Management Consultants, Farmington, NM	
111-112	Numic brownware ceramics	Great Basin (Nev. and Utah)	Desert Research Institute, Reno, NV	Rhode, 1994; Feathers and Rhode, 1998
161	Puebloan pottery	Colorado Plateau (N.Mex.)	Mariah Associates, Albuquerque, NM	
119-120	Burned sandstone (Archaic period)	Colorado Plateau (N. Mex. and Ariz.)	Navajo Nation Archaeology Department, Farmington, NM	Dykeman and Wharton, 1996; Dykeman *et al.*, 2000; Dykeman, 2000
253-254	Burned sandstone (Navajo period)			
190,192, 359-361	Puebloan pottery			
191	Burned basalt			
193-194	Basketmaker pottery			
142-147. 236-252,328-333, 357-358, 362-370, 463	Navajo pottery			
104	Burned sandstone	Colorado Plateau N. Mex.)	San Juan College, Farmington, NM	Kotyk *et al.*, undated
105-106, 303, 312	Basketmaker-Puebloan pottery			
107	Burned daub			
149-153, 302, 304-311, 313-314	Navajo pottery			
113-114, 164-166, 342-343, 372-373	Proto-historic Puebloan pottery	Chama Valley, N. Mex.	University of New Mexico, Albuquerque	Ramenofsky, 2000; Ramenofsky and Feathers, 2000
408-413	Spanish colonial ware	Comanche Springs, NM		

Entry#	Luminescence Single dates[1]	List Ref	State/Site/sherd ref.	C	P Gy	m2/m1	Procedure[2]	TotDR Gy/ka	b val Gy µm²	α %	β %	γ %	cos %	W_s %	W_e %	Z cm
68.1	1684±138 AD	WA94TLfg104	NM/LA79384/27	os	1.01±0.45	0.72±0.01	TL2;L;70°C7d;295-350°C	3.26±0.24	0.95±0.46	18.4	45.7	26.4	9.8	4	16	20
68.2	990±104 AD	WA94TLfg105	NM/LA79411/12	h	4.28±0.40	1	TL1;L;70°C30d;310-350°C	4.26±0.16	1.00±0.14	21.4	46.9	24.6	7.3	6	12	20
68.3	759±148 AD	WA94TLfg106	NM/LA79411/15	h	6.22±0.71	1	TL1;L;70°C7d;280-340°C	5.03±0.18	0.93±0.11	19.5	47.9	26.8	6	8	12	20
68.4	1556±43 AD	WA94TLfg107	NM/LA80474/30	os	2.61±0.20	1	TL1;L;70°C7d;320-360°C	5.95±0.36	1.70±0.26	34.8	36.3	23.4	5.5	7	12	10
68.5	1598±81 AD	WA94TLfg111	NV/26Ny3621/321	rs	3.32±0.68	0.83±0.01	TL1;L;70°C61d;320-360°C	8.38±0.38	0.62±0.19	20.6	47.9	27.2	4.3	0	0	32
68.6	1877±34 AD	WA94TLfg112	UT/42To13/67	rs	1.01±0.22	0.75±0.01	TL2;L;70°C7d;200-260°C	8.60±1.90	1.80±1.04	47.4	41.9	8.6	2.1	0	0	15
68.7	1432±73 AD	WA94TLfg113	NM/LA297/856	o	3.40±0.41	0.83±0.08	TL1;Q;240°C;240-340°C	6.04±0.28	1.69±0.14	36.9	47.2	9.8	6.1	11	12	0
68.8	1531±39 AD	WA94TLfg114	NM/LA297/2060	o	2.75±0.20	0.65±0.03	TL1; Q;240°C;320-380°C	5.93±0.25	1.16±0.07	27.7	54.6	11.6	6.2	11	12	0
68.9	1901±350 BC	WA94TLqi119	NM/LA71781/1073	h	15.61±1.35	1	TL1;L;180°C5m;320-350C[3]	4.01±0.10	1.96±0.76	0.7	64.1	28.9	6.2	2	6	60
68.10	1430±321 BC	WA94TLqi120	NM/LA71782/639	h	10.90±0.99	1	TL1;L;none;320-350°C	3.18±0.07	1.96±0.76	1.6	55.3	35.2	7.5	4	15	55
68.11	1654±90 AD	WA94TLfg135	NM/LA83096/230	os	2.20±0.53	0.78±0.01	TL2;L;70°C4d;280-340°C	6.46±0.73	2.21±0.78	39.8	39.2	16.6	4.5	5	16	20
68.12	1640±75 AD	WA94TLfg136	NM/LA83096/227b	os	1.94±0.31	1	TL1;L;70°C7d;250-335°C	5.48±0.77	2.11±1.20	33.9	40	20.6	5.3	4	16	20
68.13	1664±78 AD	WA94TLfg137	NM/LA83096/227a	os	1.94±0.38	1	TL1;L;70°C7d'260-350°C	5.88±0.77	2.53±1.22	37.1	38.8	19.2	4.9	3	16	20
68.14	1686±50 AD	WA94TLfg138	NM/LA83096/227c	os	2.07±0.29	0.88±0.01	TL1;L;70°C21d;230-370°C	6.72±0.56	2.28±0.60	39.4	39	17.1	4.3	5	16	20
68.15	1745±19 AD	WA95TLfg142	NM/LA105483/3	o	1.99±0.14	0.82±0.03	TL1;L;70°C5d;270-350°C	7.97±0.23	1.64±0.07	37.5	46.7	10.8	5	1	6	0
68.16	1624±32 AD	WA95TLfg143	NM/LA105530/15	o	2.59±0.21	1.12±0.05	TL1;L;70°C5d;260-310°C	6.98±0.22	1.77±0.08	37.8	45.3	11	5.7	2	6	0
68.17	1766±30 AD	WA95TLfg144	NM/LA105428/5	o	1.78±0.22	1.30±0.01	TL1;C;70°C5d;270-330°C	7.77±0.28	1.66±0.13	36	43.5	15.3	5.1	4	6	0
68.18	1665±50 AD	WA95TLfg145	NM/LA105479/1	os	1.16±0.17	1	TL1;L;70°C5d;270-320°C	3.52±0.12	0.99±0.11	14.2	58.8	15.3	11.4	1	6	0
68.19	1718±21 AD	WA95TLfg146	NM/LA105938/31	o	1.69±0.12	0.69±0.03	TL1;L;70°C7d;280-390°C	6.10±0.18	1.53±0.06	30.2	42.6	20.7	6.6	2	6	0
68.20	1734±32 AD	WA95TLfg147	NM/LA83529/1	m	1.42±0.17	1.37±0.09	TL1;L;70°C7d;270-400°C	5.44±0.18	1.69±0.11	32	48	13.1	7.4	3	6	0
68.21	1607±99 AD	WA95TLfg149	NM/LA89998/238-4	os	2.21±0.53	0.86±0.01	TL2;L;70°C21d;270-330°C	5.70±0.50	1.82±0.71	29.3	43.9	20.9	6	4	11	15
68.22	1631±39 AD	WA95TLfg150	NM/LA89998/406-4	os	2.03±0.18	1	TL1;L;70°C21d;260-300°C	5.57±0.34	1.84±0.43	31.6	42.7	19.7	6.1	4	11	15
68.23	1476±55 AD	WA95TLfg151	NM/LA89998/681-9	rf	3.18±0.24	1	TL1;L;70°C21d;260-340°C	6.13±0.45	2.30±0.59	35.6	38.7	20.2	5.5	4	11	15
68.24	1670±98 AD	WA95TLfg152	NM/LA89998/251-6	o	1.87±0.55	0.82±0.01	TL2;L;70°C21d;260-340°C	5.75±0.42	1.49±0.48	28.3	45.6	20.2	5.9	4	11	15
68.25	1736±28 AD	WA95TLfg153	NM/LA89998/268-4	o	1.39±0.13	1	TL1;L;70°C5d;270-310°C	5.34±0.29	1.74±0.37	28.8	41	23.8	6.4	5	11	15
68.26	1353±143 AD	WA95TLfg161	NM/LA100419/660	ps	3.76±0.80	0.78±0.01	TL1;L;70°C3d;300-340°C	5.86±0.42	0.90±0.35	22	59.6	14.7	3.6	5	16	125
68.27	1819±27 AD	WA95TLfg164	NM/LA298/20710	o	0.80±0.12	1	TL1;Q;240°C;320-390°C	4.55±0.19	1.43±0.13	29.5	51.4	11	8.1	7	12	0
68.28	1777±16 AD	WA95TLfg165	NM/LA298/20708	o	1.29±0.08	1	TL1;L;240°C;310-380°C	5.92±0.22	1.60±0.08	37.8	47	9	6.3	6	12	0
68.29	1854±95 AD	WA95TLfg166	NM/LA298/20703	o	0.77±0.52	na	SARA;L;240°C;310-380°C	5.47±0.22	1.40±0.15	29.8	53.4	10.2	6.8	8	12	0
68.30	881±86 AD	WA96TLfg190	AZ/I-26-23/548	m	10.6±0.65	1	TL1;C;240°C;260-290°C	9.51±0.45	1.59±0.17	44.4	43.3	10	2.3	7	20	80
68.31	4115±807 BC	WA96TLfg191	AZ/I-26-30/297	h	48.5±6.3	0.53±0.07	TL1;C;240°C;280-320°C	7.94±0.19	0.98±0.09	20.7	57.9	17.6	3.8	1	6	30
68.32	897±83 AD	WA96TLfg192	AZ/I-26-37/266	h	5.04±0.35	1.10±0.06	TL1;C; 240°C;290-310°C	4.59±0.14	1.14±0.10	19.2	49.7	25.5	5.4	3	6	16
68.33	956±94 AD	WA96TLfg193	AZ/I-25-47/515	ps	5.41±0.45	1	SARA;C;240°C;300-330°C	5.20±0.18	0.83±0.06	27.7	49.6	17.5	5.2	9	12	35
68.34	438±138 AD	WA96TLfg194	AZ/I-25-47/655	ps	12.1±0.76	1	TL1;C; 240°C;270-320°C	7.77±0.49	1.48±0.26	41.7	42.9	11.8	3.6	10	12	38
68.35	*1321±145 AD*	WA96TLfg230	AZ/U-4-4/42461	ms	2.37±0.50	0.41±0.07	TL1;L; 240°C;280-340°C	3.51±0.14	1.58±0.19	16	40.5	35.9	7.7	4	6	23
68.36	*1261±82 AD*	WA96TLfg231	AZ/U-4-33/42455A	m	2.50±0.23	1	TL1;C; 240°C;290-340°C	3.40±0.22	2.30±0.50	27.4	35.6	28.5	8.5	8	12	5
68.37	1374±58 AD	WA96TLfg232	AZ/U-4-33/42455B	m	5.18±0.43	0.76±0.03	TL1;C; 240°C;280-340°C	8.33±0.34	1.48±0.06	38.1	44.5	14	3.5	7	12	5
68.38	1308±56 AD	WA96TLfg233	AZ/U-9-41/196	ps	3.26±0.23	1	TL1;L; 240°C;320-400°C	4.74±0.19	0.86±0.04	21.9	51.5	21.1	5.5	5	6	10
68.39	*1681±26 AD*	WA97TLfg236	NM/LA106203/27	m	1.76±0.09	1	TL1;C; 240°C;290-420°C	5.57±0.19	1.56±0.04	40.6	41.1	11.1	7.2	3	6	0
68.40	1569±41 AD	WA97TLfg237a	NM/LA105475/48	o	2.10±0.16	1	SARA;L; 240°C;280-420°C	4.90±0.16	1.00±0.10	23.9	45.7	22.9	7.3	2	6	10
68.41	1489±55 AD	WA97TLfg237b	NM/LA105475/48	o	1.96±0.18	1	SARA;C; 240°C;310-400°C	3.86±0.13	1.04±0.11	16.6	45.9	28	9.3	3	6	10
68.42	1685±28 AD	WA97TLfg238	NM/LA83529/4	m	2.19±0.13	1	SARA;C; 240°C;330-410°C	7.02±0.31	1.41±0.12	34.2	45.4	15.1	5.3	2	6	9
68.43	1597±66 AD	WA97TLfg239	NM/LA79456/70	o	2.06±0.31	0.86±0.09	SARA;C; 240°C;320-400°C	5.15±0.19	1.16±0.08	27.8	42.9	21.9	7.4	3	6	8

Entry#	Luminescence Single dates	List Ref	State/Site/sherd ref.	C	P Gy	m2/m1	Procedure	TotDR Gy/ka	b val Gy μm²	α %	β %	γ %	cos %	W_s %	W_e %	Z cm
68.44	1615±38 AD	WA97TLfg240	NM/LA105630/33	m	1.70±0.14	1	TL1;C;240°C;290-340°C	4.49±0.15	1.11±0.11	24.5	47.9	18.3	8.5	2	6	9
68.45	1612±39 AD	WA97TLfg241	NM/LA105428/19	o	1.80±0.14	1	SARA;C;240°C;340-390°C	4.68±0.17	0.80±0.07	18.8	45.3	27.6	8.3	4	6	4
68.46	1661±27 AD	WA97TLfg242	NM/LA105929/20	o	1.96±0.10	1	SARA;C;240°C;350-390°C	5.84±0.21	1.12±0.05	26.4	51.9	14.9	7	3	6	0
68.47	1649±39 AD	WA97TLfg243	NM/LA110278/8	m	1.65±0.15	1	SARA;C;240°C;320-380°C	4.74±0.20	1.31±0.17	30.6	40.5	20.9	8.2	3	6	4
68.48	*1592±42 AD*	WA97TLfg244	NM/LA105930/21	m	1.54±0.13	1	SARA;C;240°C;330-390°C	3.80±0.14	1.04±0.09	24.7	40.3	25	10.3	3	6	5
68.49	*1676±22 AD*	WA97TLfg245	NM/LA106199/43	m	2.23±0.08	1	TL1;C; 240°C;240-310°C	6.94±0.21	1.31±0.07	31.6	50.6	12.2	5.6	2	6	3
68.50	*1726±24 AD*	WA97TLfg246	NM/LA106168/10	rf	1.17±0.08	0.76±0.03	TL1;C; 240°C;300-350°C	4.32±0.12	0.98±0.04	20.6	56.3	13.7	9.3	2	6	0
68.51	1491±41 AD	WA97TLfg251	NM/LA55836/8	ms	3.66±0.18	1	TL1;C; 240°C;380-420°C	7.23±0.27	1.07±0.10	34.6	49.9	9.8	5.5	3	6	0
68.52	1753±43 AD	WA97TLfg252	NM/LA55836/12	ms	1.49±0.13	0.76±0.02	TL1;C; 240°C;340-380°C	6.11±0.18	1.32±0.05	31.3	51.9	10.3	6.5	2	6	0
68.53	1535±49 AD	WA97TLqi253	NM/LA11196/389	rs	1.40±0.13	1.28±0.15	TL1;L; 240°C;300-330°C	3.03±0.11		1.7	51.8	34	12.2	1	6	10
68.54	17271± 4361 BC	WA97TLqi254	NM/LA11196/223	rf	61.2±13.3	2.33±0.59	TL1;L; 240°C;250-380°C	3.18±0.11		4.4	54.4	30.5	10.4	1	6	30
68.55	*1528±36 AD*	WA98TLfg302	NM/LA89408/2-2	o	2.25±0.15	1	TL1;C; 240°C;280-350°C	4.80±0.17	1.55±0.05	35.2	41.7	14.8	8.3	2	6	0
68.56	713±91 AD	WA98TLfg303	NM/LA89867/4-1	os	6.13±0.38	1	TL1;C; 240°C;340-370°C	4.77±0.16	0.92±0.04	23.5	50.3	18	8.4	4	6	0
68.57	*1551±33 AD*	WA98TLfg304	NM/LA89867/1-1	o	1.86±0.12	1	TL1;C; 240°C;320-390°C	4.17±0.14	1.10±0.05	23.5	47.5	19.4	9.6	3	6	0
68.58	1622±51 AD	WA98TLfg305	NM/LA112170/1-1	o	2.53±0.32	0.66±0.09	TL1;L; 240°C;310-360°C	6.75±0.33	1.05±0.15	35	44.4	14.5	5.9	3	6	0
68.59	1424±47 AD	WA98TLfg306	NM/LA114877/2-1	o	3.37±0.25	0.83±0.06	TL1;L; 240°C;330-370°C	5.87±0.21	1.47±0.08	26.7	50.1	16.2	7	4	6	0
68.60	1636±29 AD	WA98TLfg307	NM/LA89867/2-1	m	1.79±0.13	1	TL1;C; 240°C;330-380°C	4.97±0.19	1.44±0.07	32.4	46.1	13.3	8	4	6	0
68.61	1609±73 AD	WA98TLfg308	NM/LA114840/1-2	o	1.79±0.33	0.77±0.09	TL1;C; 240°C;280-390°C	4.60±0.18	1.62±0.09	34.3	41.5	16.1	8.3	3	12	0
68.62	*1681±28 AD*	WA98TLfg309	NM/LA114961/1-2	o	1.54±0.12	1	TL1;C; 240°C;320-370°C	4.86±0.21	1.65±0.17	33.7	42.8	15.2	8.4	3	6	0
68.63	1703±22 AD	WA98TLfg310	NM/LA114962/1-1	o	1.32±0.09	0.90±0.03	TL1;C; 240°C;240-350°C	4.48±0.15	1.41±0.04	30.4	46.2	14.1	9.2	3	6	0
68.64	1739±23 AD	WA98TLfg311	NM/LA112170/2-1	o	1.62±0.13	0.82±0.04	TL1;C; 240°C;300-370°C	6.26±0.23	1.76±0.08	37.7	42	13.9	6.4	3	6	0
68.65	638±139 AD	WA98TLfg312	NM/LA114932/2-2	m	6.76±0.51	1	TL1;L; 240°C;350-370°C	4.97±0.21	1.28±0.14	33.6	44.1	14.3	8.2	3	6	0
68.66	1679±58 AD	WA98TLfg313	NM/LA112171/8-2	m	1.30±0.23	1	TL1;L; 240°C;320-370°C	4.07±0.18	1.36±0.14	29	45	16.2	9.8	4	6	0
68.67	1716±29 AD	WA98TLfg314	NM/LA114932/4-2	m	1.57±0.15	0.70±0.05	TL1;L; 240°C;300-350°C	5.57±0.24	1.80±0.10	40.8	37.2	14.7	7.4	4	6	0
68.68	1448±64 AD	WA98TLfg328	NM/LA79469/280	o	4.08±0.44	1.59±0.13	TL1;L; 240°C;340-400°C	7.42±0.31	1.97±0.18	39.6	40.3	15.1	5	2	6	10
68.69	1596±31 AD	WA98TLfg329	NM/LA79469/335	os	3.49±0.24	1	TL1;C; 240°C;330-380°C	8.69±0.28	1.95±0.07	42.9	41.7	11.3	4.3	2	6	10
68.70	1606±45 AD	WA98TLfg330	NM/LA78178/88	os	3.10±0.33	0.74±0.05	TL1;C; 240°C;250-310°C	7.91±0.37	2.06±0.16	48.8	31.6	15.7	4	3	6	30
68.71	1646±42 AD	WA98TLfg331	NM/LA78178/174	m	1.61±0.18	1.30±0.13	TL1;L; 240°C;250-310°C	4.57±0.18	2.31±0.15	39.2	33.5	20.8	6.6	2	6	40
68.72	1387±103 AD	WA98TLfg332	NM/LA78178/328	os	4.67±0.77	1	TL1;L; 240°C;230-390°C	7.64±0.29	1.61±0.13	37.6	43.1	15.3	3.9	3	6	40
68.73	1707±29 AD	WA98TLfg333	NM/LA78178/112	m	1.99±0.18	0.74±0.08	TL1;L; 240°C;300-380°C	6.84±0.28	1.54±0.15	37.6	41.1	16.5	4.8	3	6	20
68.74	1578±51 AD	WA98TLfg342	NM/LA908/35068	o	3.09±0.33	0.66±0.06	TL1;L; 240°C;260-320°C	7.35±0.44	1.56±0.15	38.1	48	8.8	5.2	8	12	0
68.75	1323±125 AD	WA98TLfg343	NM/LA908/35058	o	4.00±0.70	0.45±0.08	TL1;L; 240°C;300-410°C	5.93±0.35	1.28±0.26	31.2	51.8	10.6	6.4	9	12	0
68.76	1503±42 AD	WA98TLfg344	CO/5MN4270/211	o	3.45±0.19	0.84±0.05	TL1;L; 240°C;310-370°C	6.97±0.26	1.56±0.08	37.3	44.8	12.6	5.3	4	12	3
68.77	1411±84 AD	WA98TLfg345	CO/5MN4253/4209	o	2.64±0.34	na	SARA; 240°C;240-320°C	4.50±0.20	1.41±0.13	31.3	44.2	16.7	8	4	12	6
68.78	1576±68 AD	WA98TLfg346	CO/5ME4970/247	h	2.01±0.27	na	SARA; 240°C;300-380°C	4.77±0.34	1.54±0.29	30.2	39.4	22.6	7.8	3	12	4
68.79	961±110 AD	WA98TLfg347	CO/5MN4270/222	o	7.37±0.63	na	SARA; 240°C;280-380°C	7.11±0.26	1.71±0.08	39.4	42.9	12.5	5.1	4	12	5
68.80	*1778±33 AD*	WA98TLfg348	CO/5MN4253/254	o	1.01±0.13	na	SARA; 240°C;260-340°C	4.59±0.24	1.46±0.09	31.2	44.9	16.3	7.6	4	12	8
68.81	1616±36 AD	WA98TLfg349	NM/LA86094/208	o	1.98±0.12	0.67±0.03	TL1;C;240°C;320-410°C	5.18±0.24	2.08±0.10	34.2	44.4	14.7	6.9	4	12	4
68.82	1714±45 AD	WA98TLfg350	CO/5MN4253/240	o	1.45±0.20	na	SARA;240°C;270-350°C	5.11±0.32	1.71±0.28	36.4	43.1	13.7	7	4	12	6
68.83	1509±53 AD	WA98TLfg351	CO/5MN2628/255	o	2.09±0.18	na	SARA;240°C;280-380°C	4.27±0.17	1.71±0.09	26.9	45	19.2	8.9	3	12	15
68.84	*1678±32 AD*	WA99TLfg357	NM/LA55979/1987	os	2.14±0.02	0.81±0.05	TL1;Q; 240°C;300-400°C	6.66±0.23	1.83±0.08	37.1	39	18.8	5.1	3	6	20
68.85	1567±30 AD	WA99TLfg358	NM/LA55979/2626	o	2.78±0.17	1	TL1;Q; 240°C;340-390°C	6.44±0.20	1.59±0.07	34.2	42.5	18.2	5.3	3	6	20
68.86	788±90 AD	WA99TLfg359	NM/LA55979/985	ps	7.35±0.47	1	TL1;Q; 240°C;290-410°C	6.08±0.23	1.50±0.07	31.9	43.4	20.7	3.9	3	6	150

Entry#	Luminescence Single dates	List Ref	State/Site/sherd ref.	C	P Gy	m2/m1	Procedure	TotDR Gy/ka	b val Gy μm^2	α %	β %	γ %	cos %	W_s %	W_e %	Z cm
68.87	1157±77 AD	WA99TLfg360	NM/LA55979/1036	ps	4.54±0.38	0.84±0.04	TL1;Q;240°C;270-310°C	5.39±0.20	1.67±0.05	33.6	40.6	21.3	4.5	3	6	150
68.88	1021±68 AD	WA99TLfg361	NM/LA55979/1035	ps	5.47±0.33	1	TL1;Q;240°C;280-300°C	5.60±0.19	1.65±0.06	31.4	40.5	23.4	4.3	3	6	150
68.89	1510±39 AD	WA99TLfg362	NM/LA55979/2218	os	2.20±0.16	1.22±0.07	TL1;Q;240°C;270-400°C	4.50±0.16	1.32±0.05	22.2	47.3	22.7	7.6	4	6	20
68.90	1591±31 AD	WA99TLfg363	NM/LA55979/2299	os	2.57±0.17	1	TL1;Q;240°C;300-370°C	6.30±0.23	1.77±0.07	35.9	41.9	17	5.4	3	6	20
68.91	1557±41 AD	WA99TLfg364	NM/LA55979/2413	os	2.36±0.20	0.87±0.05	TL1;Q;240°C;320-380°C	5.34±0.18	1.79±0.07	32	42.3	19.1	6.4	3	6	20
68.92	1627±31 AD	WA99TLfg365	NM/LA55979/3205	os	1.56±0.07	1	TL1;Q;240°C;340-380°C	5.27±0.18	1.96±0.15	28.8	46.1	18.6	6.5	4	6	20
68.93	1552±44 AD	WA99TLfg366	NM/LA55979/3101	os	3.05±0.27	1	TL1;Q;240°C;285-385°C	6.82±0.28	1.30±0.11	37.1	40.3	17.6	5	4	6	20
68.94	1559±51 AD	WA99TLfg367	NM/LA55979/1889	os	2.06±0.22	0.85±0.06	TL1;Q;240°C;260-400°C	4.68±0.21	1.51±0.09	24.8	45.1	23.1	7.3	3	6	20
68.95	1619±42 AD	WA99TLfg368	NM/LA55979/2762	os	1.92±0.20	0.66±0.05	TL1;Q;240°C;280-410°C	5.05±0.20	1.71±0.09	34.9	40.6	17.8	6.7	4	6	20
68.96	1527±39 AD	WA99TLfg369	NM/LA55979/2601	os	2.70±0.20	1	TL1;Q;240°C;320-400°C	5.72±0.21	1.70±0.07	32.7	42.1	19.1	5.9	2	6	20
68.97	1626±34 AD	WA99TLfg370	NM/LA55979/2649	os	2.00±0.16	0.75±0.05	TL1;L;240°C;260-420°C	5.37±0.24	1.64±0.10	33.1	40.2	20.3	6.3	4	6	20
68.98	1680±27 AD	WA99TLfg372	NM/LA908/35062	o	2.08±0.15	1	TL1;L;240°C;310-360°C	6.55±0.30	1.68±0.14	35.6	49.6	9	5.8	10	12	0
68.99	1552±35 AD	WA99TLfg373	NM/LA298/20707	o	2.93±0.19	1	TL1;Q;240°C;280-320°C	6.57±0.29	1.72±0.09	38.8	47.3	8.4	5.6	10	12	0
68.100	*1713±27 AD*	WA00TLfg408	NM/LA14904/fs219	ms	1.44±0.12	1	TL1;Q;240°C.290-360°C	5.03±0.20	1.83±0.12	36.3	41.2	16.6	5.9	7	12	24
68.100	1666±27 AD	WA00TLfg409	NM/LA14904/fs237	ms	1.53±0.11	1	TL1;Q;240°C.300-390°C	4.58±0.16	1.63±0.06	31.3	44.2	18.3	6.2	7	12	30
68.102	*1805±34 AD*	WA00TLfg410	NM/LA14904/fs225	ms	0.87±0.15	0.78±0.06	TL1;L;240°C.320-400°C	4.45±0.16	1.53±0.08	28.5	45.6	19.4	6.5	7	12	26
68.103	1683±32 AD	WA00TLfg411	NM/LA14904/f5117	ms	1.26±0.11	0.88±0.04	TL1;L;240°C.250-400°C	3.98±0.20	2.26±0.13	37.6	34.0	21.0	7.4	6	12	25
68.104	1655±28 AD	WA00TLfg412	NM/LA14904/fs231	ms	1.71±0.12	1	TL1;Q;240°C.320-400°C	4.98±0.21	1.98±0.16	36.5	41.6	15.6	6.3	7	12	15
68.105	*1850±15 AD*	WA00TLfg413	NM/LA14904/fs265	ms	1.03±0.09	0.74±0.05	TL1;L;240°C.260-340°C	6.91±0.30	1.71±0.10	37.8	44.1	13.5	4.5	8	12	15
68.106	1619±50 AD	WA00TLfg430	CO/5SM2425/2204	o	1.77±0.20	1	SARA;L;240°C;240-400°C	4.59±0.23	1.75±0.21	27.5	50.8	15.0	6.5	10	12	15
68.107	1654±37 AD	WA00TLfg463	NM/LA16257fs547	os	2.04±0.20	0.82±0.05	TL1;Q;240°C.310-400°C	5.90±0.23	1.71ë0.09	35.8	39.1	19.1	6.0	7	9	18

Notes.

1. Dates in italics are for samples that exhibited anomalous fading and can only be considered minimums. In addition, fading tests were not conducted on a number of sherds, due to insufficient material. These are sherd references: 137, 150, 151, 237a, 238b, 243, 308, 313, 332, 345, 346, 347, 350, 366, 368
2. For the five samples for which TL2 procedure (additive dose extrapolation with supralinearity correction) was followed, the ratio of the second glow intercept to the palaeodose was as follows: #104 (0), #112 (0), #135 (0.16±0.15), #149 (0.09±0.07), #152 (0.05±0.04).
3. For #119, a piece of burned sandstone, OSL was performed as well as TL, and the data reflect weighted averages of both analyses.

Abbreviations

4. List Ref includes the laboratory (WA, or University of Washington), year of analysis, TL or OSL, fine grain (fg) or quartz inclusion (qi), and the laboratory reference number.
5. The column headed by C gives the archaeological context of the sample: pit structure (ps), masonry structure (ms), other kind of structure (os), hearth (h, any feature with carbonized material), rockshelter (rs), rock feature (rf, any small feature constructed with stones, such as mealing bins), midden (m), and other (o, generalized activity areas of habitation sites).
6. P is palaeodose in Gy.
7. m2/m1 is the ratio of slopes of the regeneration and additive dose curves.
8. Procedure includes the basic procedure for determining palaeodose (as referenced in Table 1), fit to the growth curves (L, linear, Q, quadratic, C, cubic), preheat, and plateau region.
9. TotDR is the total dose rate. This is followed by the b-value, and the percent dose rate of alphas, betas, gammas, and cosmic. W refers to moisture contents of sample and environment. Z is the burial depth.

Obituary

Galina Hütt (1937 - 2000)

Galina Hütt was born 17 February 1937 in Odessa (Ukrainia, then SSR), she was the daughter of Isaak Koz.

Her higher education was in 'pure' Physics: In 1954, she started her University studies in the Department of Physics of Tartu University (Estonia, then SSR), the "Oxford" of Estonia, where she was to stay until 1974. After graduation (in 1959), she was briefly high school teacher, then in the Institute of Physics of Estonian Academy of Sciences, as a researcher in the Department of Radiation Physics. She was awarded in 1972 the title of 'Candidate in Physics' (that is equivalent to Ph.D.) at Tartu University for her work:
"The study of microstructure of defects in calcium sulphide", Dr Ivar Jaek being her supervisor .

In 1974, she started working in the Institute of Geology of Estonian Academy of Sciences, shifting from luminescence studies to more applied thermoluminescence Dosimetry and Dating. She started to participate to International Scientific life (Oxford Seminar, 1978 etc.) in so far as was possible in USSR at the time. Her major study in this field was made at the Dating Seminar in Cambridge, (1987), it was actually a contribution of physics of luminescence to Dosimetry:
"G.Hütt, I.Jaek, J.Tchonka (1988) Optical dating: K-feldspars optical response stimulation spectra. Quaternary Science Reviews, 7, 381-385.).
This is known now as the method of IRSL. It was first received with strong scepticism, before becoming a standard method for feldspar TL dating.

In 1986, she became head of the 'Paleodosimetry Laboratory' in the Institute of Geology of the Estonian Academy of Sciences, which she set up with proper equipment and staffed with a competent team of scientists.

In 1990, she became 'Doctor in Physics' at Latvian State University (Riga), (title equivalent to what is known in some countries as 'Habilitation' to apply for a Professorship). Meanwhile, she had a very important scientific activity, witnessed by many publications. It is impossible to quote here all her studies, some 100 articles dealing with other fundamental studies of luminescence of materials and minerals, dating of sediments, accident paleodosimetry (Chernobyl, Kiisa), over all these years up to the last meeting in Rome (1999). These studies have been conducted with her colleagues from Estonia, but also from Finland, Germany, Great Britain etc.

Her life was not made easy by circumstances, political or others : From her younger age, when she remembered fleeing from Odessa in 1941 under Nazi bombing; sharing all the upheavals of Estonia, her adoptive country recovering independence during these years; a very bad accident which left her getting around on crutches for years, not to mention her dramatic murder.

All her achievements above mentioned, such as setting up a laboratory of international standard, could be accounted for by the strong resolution of Galina. She was a lady of a rather steadfast and unwavering nature, a formidable opponent in scientific debates, who managed to get things done against all obstacles.
But she was also a very kind person. Most people who worked with her became her friends and have a feeling of sadness thinking of the small laboratory way north in Tallinn, and the nice time spent there.

Raphaël Visocekas

Thesis abstract

Thesis title: pulsed optical stimulation of luminescence from quartz
Author: Makaiko Chitchambo
Date: 2000
Supervisor: Dr. R.B. Galloway
University: The university of Edinburgh, Dept. of Physics and Astronomy

A light emitting diode based pulsing system capable of producing luminescence time-resolved spectra was developed for study of optically stimulated luminescence from quartz and feldspar. The aim of the pulsed optical stimulation method is to separate in time stimulation and detection of luminescence so that luminescence can be measured in the absence of scatter from stimulating light unlike in conventional continuous stimulation where luminescence monitored includes such scatter. Pulsed optical stimulation not only offers the possibility of improvements in signal to background ratio but also the ability to investigate the time dependence of luminescence emission relative to the time of stimulation. Although study of pulsed luminescence has been dominated by laser-based systems, a pulsing system based on light emitting diodes offers, in comparison, advantages of simplicity and economy.

The present system has been used over a wide range of pulse widths (25 ns (FWHM) - 30 μs) and dynamics ranges (40 ns - 64 μs). The system can be adapted for use with a wide range of wavelengths with pulse widths from 25 ns (FWHM) to as long as desired.

Luminescence time-resolved spectra have been recorded from feldspar and quartz. Half lives measured from feldspar range from 25 ns and from quartz, 20 - 28 μs. Properties of luminescence half lives from quartz were studied in detail as a function of experimental parameters such as stimulation time, temperature, radiation dose, and preheating method. The influence of temperature on luminescence intensity was studied for time-resolved spectra recorded at long stimulation times. Explanations rare proposed to account for experimental results.

Bibliography

(From 1st June 2000 to 20th September 2000) Compiled by Ann Wintle

Aitken M. J. (1999) Archaeological dating using physical phenomena. *Reports on Progress in Physics* **62**, 1333-1376.

Barnett S. M. (2000) Luminescence dating of pottery from later prehistoric Britain. *Archaeometry* **42**, 431-457.

Bensimon Y., Deroide B., Dijoux F., and Martineau M. (2000) Nature and thermal stability of paramagnetic defects in natural clay: a study by electron spin resonance. *Journal of Physics and Chemistry of Solids* **61**, 1623-1632.

Berger G. W. and Anderson P. M. (2000) Extending the geochronometry of Arctic lake cores beyond the radiocarbon limit by using thermoluminescence. *Journal of Geophysical Research - Atmospheres* **105**, 15439-15455.

Cechak T., Gerndt J., Kubelik M., Musilek L., and Pavlik M. (2000) Radiation methods in research of ancient monuments. *Applied Radiation and Isotopes* **53**, 565-570.

Chitambo M. L. and Galloway R. B. (2000) A pulsed light-emitting-diode system for stimulation of luminescence. *Measurement Science and Technology* **11**, 418-424.

Cook G. D., Price D. M., and Woodroffe C. D. (2000) Late Quaternary alluviation along intermittent streams in Kakadu National Park, Northern Territory. *Australian Geographer* **31**, 155-162.

Costantini J. M., Brisard F., Biotteau G., Balanzat E., and Gervais B. (2000) Self-trapped exciton luminescence induced in alpha quartz by swift heavy ion irradiations. *Journal of Applied Physics* **88**, 1339-1345.

El-Asmar H. M. and Wood P. (2000) Quaternary shoreline development: the northwestern coast of Egypt. *Quaternary Science Reviews* **19**, 1137-1149.

Gillespie R. and Roberts R. G. (2000) On the reliability of age estimates for human remains at Lake Mungo. *Journal of Human Evolution* **38**, 727-732.

Grün R. and Schwarcz H. P. (2000) Revised open system U-series/ESR age calculations for teeth from Stratum C at the Hoxnian Interglacial type locality. *Quaternary Science Reviews* **19**, 1151-1154.

Grün R., Spooner N. A., Thorne A., Mortimer G., Simpson J. J., McCulloch M. T., Taylor L., and Curnoe D. (2000) Age of the Lake Mungo 3 skeleton, reply to Bowler & Magee and to Gillespie & Roberts. *Journal of Human Evolution* **38**, 733-741.

Grün R., Tani A., Gurbanov A., Koschug D., Williams I., and Braun J. (1999) A new method for the estimation of cooling and denudation rates using paramagnetic centers in quartz: a case study on the Eldzhurtunskiy Granite, Caucasus. *Journal of Geophysical Research - Solid Earth* **104**, 17531-17549.

Hashimoto T., Takano M., Yanagawa Y., and Tsuboi T. (2000) Radiation dosimetry using thermoluminescence from ceramic and glass samples at the JCO critical accident site. *Journal of Environmental Radioactivity* **50**, 97-105.

Hong D. G., Galloway R., and Hashimoto T. (2000) Additive dose single and multiple aliquot methods of equivalent dose determination compared for quartz luminescence stimulated by green light. *Japanese Journal of Applied Physics* **39**(7A), 4209-4216.

Juyal N., Raj R., Maurya D. M., Chamyal L. S., and Singhvi A. K. (2000) Chronology of Late Pleistocene environmental changes in the lower Mahi basin, western India. *Journal of Quaternary Science* **15**, 501-508.

Kailath A. J., Rao T. K. G., Dhir R. P., Nambi K. S. V., Gogte V. D., and Singhvi A. K. (2000) Electron spin resonance characterization of calcretes from Thar desert for dating applications. *Radiation Measurements* **32**, 371-383.

Kale V. S., Singhvi A. K., Mishra P. K., and Banerjee D. (2000) Sedimentary records and luminescence chronology of Late Holocene palaeofloods in the Luni River, Thar Desert, northwest India. *Catena* **40**, 337-358.

Kawaguchi Y. (1999) Fractoluminescence in minerals. *Radiation Effects and Defects in Solids* **149**, 131-135.

Mercier N., Valladas H., Froget L., Joron J. L., and Ronen A. (2000) TL dating of the lowest Paleolithic deposits of the Tabun Cave (Mt. Carmel, Israel). *Comptes Rendus de l'Académie des Sciences* **330**, 731-738.

Michael C. T. and Zacharias N. (2000) A new technique for thick source alpha counting determination of U and Th. *Nuclear Instruments and Methods in Physics Research A* **439**, 167-177.

Munro R. N., Morgan R. V. H., and Jobling W. J. (1997) Optical dating and landscape chronology at ad-Disa, Southern Jordan, and its potential. *Studies in the history and archaeology of Jordan* **VI**, 97-103.

Munyikwa K., Van den Haute P., Vandenberghe D., and De Corte F. (2000) The age and palaeoenvironmental significance of the Kalahari Sands in western Zimbabwe:a thermoluminescence reconnaissance study. *Journal of African Earth Sciences* **30**, 941-956.

Olley J. and Caitcheon G. (2000) Major element chemistry of sediments from the Darling-Barwon River and its tributaries: implications for sediment and phosphorus sources. *Hydrological Processes* **14**, 1159-1175.

Poolton N. R. J., Smith G. M., Riedi P. C., Bulur E., Bøtter-Jensen L., Murray A. S., and Adrian M. (2000) Luminescence sensitivity changes in natural quartz induced by high temperature annealing: a high frequency EPR and OSL study. *Journal of Physics D - Applied Physics* **33**, 1007-1017.

Richter D., Waiblinger J., Rink W. J., and Wagner G. A. (2000) Thermoluminescence, electron spin resonance and C-14-dating of the Late Middle and Early Upper Palaeolithic site of Geissenklosterle Cave in southern Germany. *Journal of Archaeological Science* **27**, 71-89.

Sanzelle S., Pilleyre T., Montret M., Faïn J., Miallier D., Camus G., de Hervé A. D., and Defleur A. (2000) Thermoluminescence dating: study of a possible chronological correlation between the maar of La Vestide-du-Pal and a tephra layer from La Baume-Moula-Guercy (Ardèche, France). *Comptes Rendus de l'Académie des Sciences Série II* **330**, 541-546.

Schwarcz H. P. and Rink W. J. (2000) ESR dating of the Die Kelders archaeological site. *Journal of Human Evolution* **38**, 121-128.

Tanir G., Arikan N., Sarer B., and Tel E. (2000) The application of the IRSL dating technique to feldspars from Kayseri-Turkey. *Journal of Environmental Radioactivity* **51**, 363-370.

Trukhin A. N., Fitting H. J., Bafels T., and von Czarnowski A. (1999) Cathodoluminescence and IR absorption of oxygen deficient silica - influence of hydrogen treatment. *Radiation Effects and Defects in Solids* **149**, 61-68.

Vanhaelewyn G., Callens F., and Grün R. (2000) EPR spectrum deconvolution and dose assessment of fossil tooth enamel using maximum likelihood common factor analysis. *Applied Radiation and Isotopes* **52**, 1317-1326.

Wallinga J. and Duller G. A. T. (2000) The effect of optical absorption on the infrared stimulated luminescence age obtained on coarse-grain feldspar. *Quaternary Science Reviews* **19**, 1035-1042.

Wu Z., Wang W., Tan H. H., and Xu F. Y. (2000) The age of the "old red sand" on the coasts of south Fujian and west Guangdong, China. *Chinese Science Bulletin* **45**, 1216-1221.

Zöller L. (2000) Chronology of upper Pleistocene "red silts" in the Siwalik system and constraints for the timing of the upper palaeolithic in Nepal. *Catena* **41**, 229-235.